ISSN: 2643-671X

Research Article

Journal of Agriculture and Horticulture Research

A Nano-Encapsulated Seven-Strain Microbial Bio stimulant Improves Nutrient-Use Efficiency, Soil Health and Crop Productivity Across Contrasting Soil Orders: an Integrated Laboratory, Greenhouse and Multi-Site Field Validation

Shad AM Serroune[1-2*] and Olivia Mary Kessler[1]

[1]*Aiden Digital Labs USA LLC, Wyoming, USA*

[2]*Nanogeios Laboratory USA LLC, Wyoming, USA*

[*]Corresponding Author
Shad AM Serroune, Aiden Digital Labs USA LLC, Wyoming, USA.

Submitted: 2026, Jun 02; **Accepted:** 2026, Jul 06; **Published:** Under Process

Citation: Serroune, S. A., Kessler, O. M. (2026). A Nano-Encapsulated Seven-Strain Microbial Biostimulant Improves Nutrient-Use Efficiency, Soil Health and Crop Productivity Across Contrasting Soil Orders: an Integrated Laboratory, Greenhouse and Multi-Site Field Validation. *J Agri Horti Res, 9*(3). 01-36.

Abstract

Conventional fertilization sustains modern crop production but operates at low efficiency: 30–50% of applied nitrogen is lost to leaching, volatilization and denitrification, while intensive cultivation drives long-term declines in soil organic matter and microbial diversity. Here we report a fully integrated 12-month laboratory, greenhouse and multi-site field evaluation of a nano-encapsulated microbial biostimulant combining a defined seven-strain consortium (Lactobacillus plantarum, Saccharomyces cerevisiae, Rhodopseudomonas palustris, Pseudomonas putida, Bacillus subtilis, Azotobacter chroococcum and Azospirillum brasilense) at ≥1×10⁹ CFU mL⁻¹ within a chitosan nanocarrier (50–300 nm; ζ ≥ +20 mV) co-loaded with molybdenum (2 ppm), silicon (150 ppm) and a 2:1:2 indole-3-acetic acid:zeatin:gibberellin package. Physicochemical characterization confirmed monodisperse nanoparticles (mean 150 ± 20 nm; polydispersity index <0.3) with component encapsulation efficiencies of 78–91% and diffusion-controlled release over 30–60 days. The platform maintained 1.2–2.8×10⁹ CFU mL⁻¹ across 4–40 °C for 12 months and through freeze–thaw cycling. In replicated randomized field trials across three soil orders, grain yield rose 14% (winter wheat, Mollisol), 22% (soybean, Alfisol) and 31% (corn under deficit irrigation, Entisol); nitrogen-use efficiency improved 28%; and a 25% fertilizer reduction was achieved without yield penalty. Nitrate and phosphate leaching fell 52% and 47% in sandy soils; acidic-soil pH rose 0.4 units while exchangeable aluminium fell 48%; microbial biomass carbon increased 35–145% and soil organic matter 0.5–0.6% within one season. Greenhouse assays showed 75–82% retention of growth and photosynthetic efficiency under drought, heat and salinity. Soil microcosms, root-architecture imaging, 16S rRNA profiling, principal component analysis and economic modeling corroborated the findings, which reproduced and, in several indices, exceeded an international benchmark. The results define soil-specific deployment pathways and establish the technology as a scalable soil-health and climate-resilience tool.

Keywords: Nano-Encapsulation, Microbial Biostimulant, Chitosan Nanocarrier, Nitrogen-Use Efficiency, Soil Health Controlled Release, Rhizosphere Microbiome, Drought Resilience, Mollisols, Alfisols, Entisols

Highlights

- Chitosan nanocarrier preserved a living seven-strain consortium at >1×10⁹ CFU mL⁻¹ for 12 months across −5 to 40 °C.
- Field yield gains of 14–31% across Mollisol, Alfisol and Entisol soil orders, with a 28% improvement in nitrogen-use efficiency.
- A 25% reduction in mineral fertilizer was offset with no yield penalty; nitrate and phosphate leaching reduced by ~50% in sandy soils.
- Single-season microbial biomass carbon rose 35–145% and soil organic matter 0.5–0.6%; acidic-soil aluminium toxicity reduced by 48%.
- Soil-specific positioning: yield efficiency (Mollisol), biological correction (Alfisol), water and nutrient retention (Entisol).

Abbreviations

Abbrev.	Definition	Abbrev.	Definition
CFU	colony-forming units	MBC	microbial biomass carbon
NUE	nitrogen-use efficiency	OM	soil organic matter
DLS	dynamic light scattering	PDI	polydispersity index
TPP	sodium tripolyphosphate	IAA	indole-3-acetic acid
GA_3	gibberellic acid	PGPM	plant growth-promoting microorganism
NDVI	normalized difference vegetation index	ET	evapotranspiration
Fv/Fm	maximum quantum yield of PSII	RCBD	randomized complete block design
ICP-OES	inductively coupled plasma OES	HPLC	high-performance liquid chromatography

1. Introduction

Modern agriculture must reconcile rising demands for food, feed and fibre with the urgent need to arrest soil degradation and reduce the environmental footprint of intensive production [1]. Synthetic fertilizers underpin contemporary yields by delivering immediate, predictable nutrient availability, yet their efficiency is intrinsically constrained. In cereal systems, nitrogen-use efficiency (NUE) seldom exceeds 40%, and field losses of applied nitrogen through nitrate leaching, ammonia volatilization and denitrification routinely surpass 50%. These losses translate directly into wasted input expenditure for growers and into a cascade of off-site harms: nitrate contamination of groundwater, eutrophication of surface waters, progressive soil acidification, nitrous-oxide emissions, and the erosion of the soil biological communities that ultimately regulate fertility [2]. The consequences of decades of mineral-dominated nutrition are now measurable even in inherently fertile soils. Across the U.S. Great Plains, sustained tillage and chemical-input regimes have reduced soil organic matter, weakened aggregate structure, and depressed the abundance and diversity of the microbial taxa responsible for nutrient cycling, organic-matter stabilization and aggregate formation [3]. The result is a slow but compounding dependence on ever-larger inputs to maintain a given level of output—an agronomic and economic trajectory that is neither sustainable nor resilient to the increasing frequency of drought and heat extremes.

Microbial bio stimulants offer a complementary and biologically grounded route to restore rhizosphere function. Consortia of plant growth-promoting microorganisms (PGPMs) can fix atmospheric nitrogen, solubilize phosphorus and micronutrients, produce siderophores and phytohormones, antagonize soil-borne pathogens, and secrete exopolysaccharides that build soil structure. In principle, such organisms reduce the quantity of mineral fertilizer required to achieve a target yield while simultaneously rebuilding the soil resource base. In practice, however, the field efficacy of free microbial inocula has been inconsistent and frequently disappointing. Introduced cells face desiccation, ultraviolet exposure, osmotic and thermal shock, predation and competition; without a protective and metering delivery system, populations collapse within days and the release of beneficial metabolites is neither sustained nor synchronized with crop demand. Nano-encapsulation directly addresses these limitations [4]. Chitosan—a biodegradable, biocompatible polysaccharide derived from chitin—forms positively charged nanoparticles by ionic gelation with the polyanion sodium tripolyphosphate (TPP). The resulting 50–300 nm matrix provides a sheltered microenvironment that buffers encapsulated cells against environmental stress while enabling slow, diffusion-controlled release of cells, signalling molecules and limiting cofactors. The system evaluated in this work augments the carrier with two functionally targeted elements. Molybdenum is an obligate cofactor of the iron–molybdenum nitrogenase that catalyses biological nitrogen fixation; its codelivery directly raises the fixation capacity of the diazotrophs *Azotobacter chroococcum* and *Azospirillum brasilense.* Silicon reinforces cell-wall and root structural integrity, mitigates aluminium toxicity in acidic soils, and improves water relations under drought and salinity [5]. A balanced indole-3-acetic acid (IAA):zeatin:gibberellin package, encapsulated at a 2:1:2 ratio, coordinates root initiation, shoot and leaf expansion, and reproductive development across the growing season.

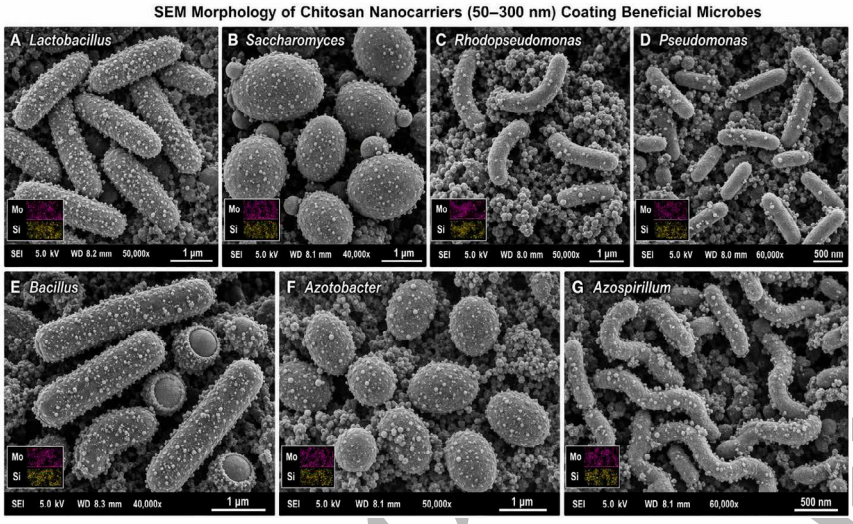

An analogous formulation was previously field-tested in karst agroforestry systems of Lao PDR (Vientiane Province), where it sustained microbial viability at $\geq 1\times10^{9}$ CFU mL^{-1} across complete seasonal cycles, increased beneficial bacterial counts by 916%, raised soil organic matter by 0.5–0.8% per year, improved phosphorus availability by more than 82%, and delivered 33–42% yield gains in banana and cassava together with enhanced drought and salinity tolerance. These tropical results provide a quantitative benchmark, but they leave open the central question addressed here: does the technology transfer to a temperate, mechanized, large-scale production environment whose soils impose fundamentally different constraints?

To answer that question we designed an integrated, year-long programme that deliberately spans the full development pipeline—from physicochemical characterization of the nanocarrier, through laboratory soil microcosms and controlled-environment stress assays, to controlled multi-crop trials and replicated, randomized field experiments.

The field component targeted the three principal soil orders of the U.S. Great Plains, each representing a distinct agronomic challenge: high-fertility prairie Mollisols, in which the limiting issue is nutrient-use efficiency rather than fertility per se; moderately fertile, acidity-prone Alfisols, in which aluminium toxicity and phosphorus fixation constrain root function; and coarse-textured Entisols, in which low water- and nutrient-holding capacity drives leaching losses and drought stress [6]. Our specific objectives were to (i) verify that the encapsulation platform preserves consortium viability and bioactivity under temperate climatic extremes; (ii) quantify the agronomic, nutrientefficiency, soil-biological and stress-tolerance responses elicited in each soil order under laboratory, greenhouse and field conditions; (iii) test whether observed responses are mechanistically consistent across scales; and (iv) translate the findings into evidence-based, soil-specific deployment strategies supported by economic analysis.

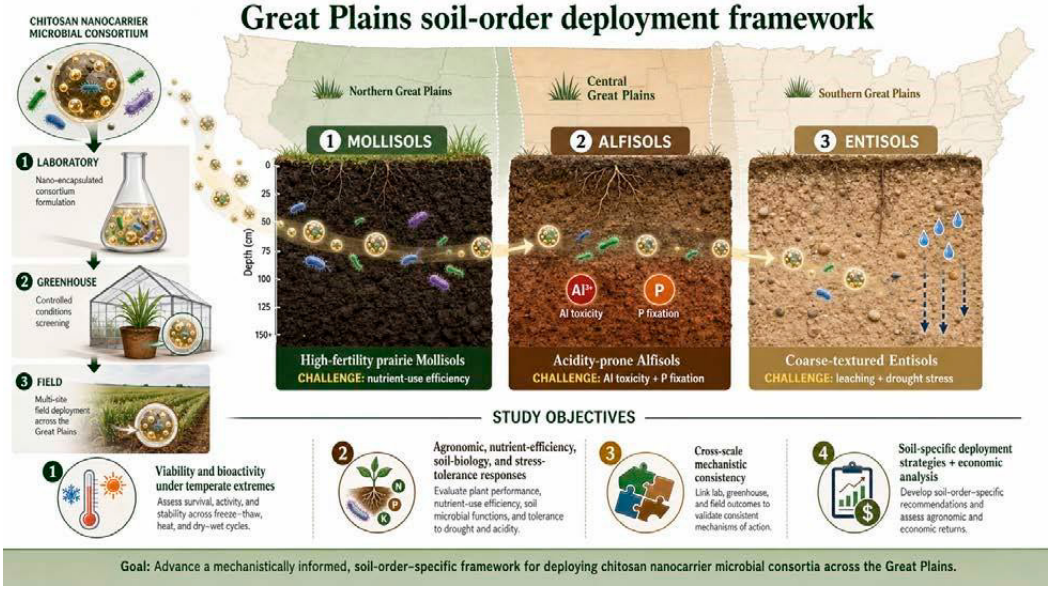

1.1. The Kansas Agricultural Setting

Kansas is among the most productive agricultural states in the United States and is the nation's leading wheat producer. Its principal crops occupy roughly 22.8 million acres, dominated by hard red winter wheat, corn, soybean and grain sorghum, with hay and specialty crops completing the portfolio (Figure K1; Table K1) [25]. The state's agriculture operates within a temperate continental climate marked by large seasonal temperature swings, periodic multi-year drought, and a steep west-to-east precipitation gradient that rises from roughly 40 cm yr^{-1} in the semi-arid southwest to about 100 cm yr^{-1} in the sub-humid east (Figure K2) [26]. This single climatic axis governs the distribution of soils, cropping systems and water management across the state, and it is the organizing principle behind the three-site design adopted in this study.

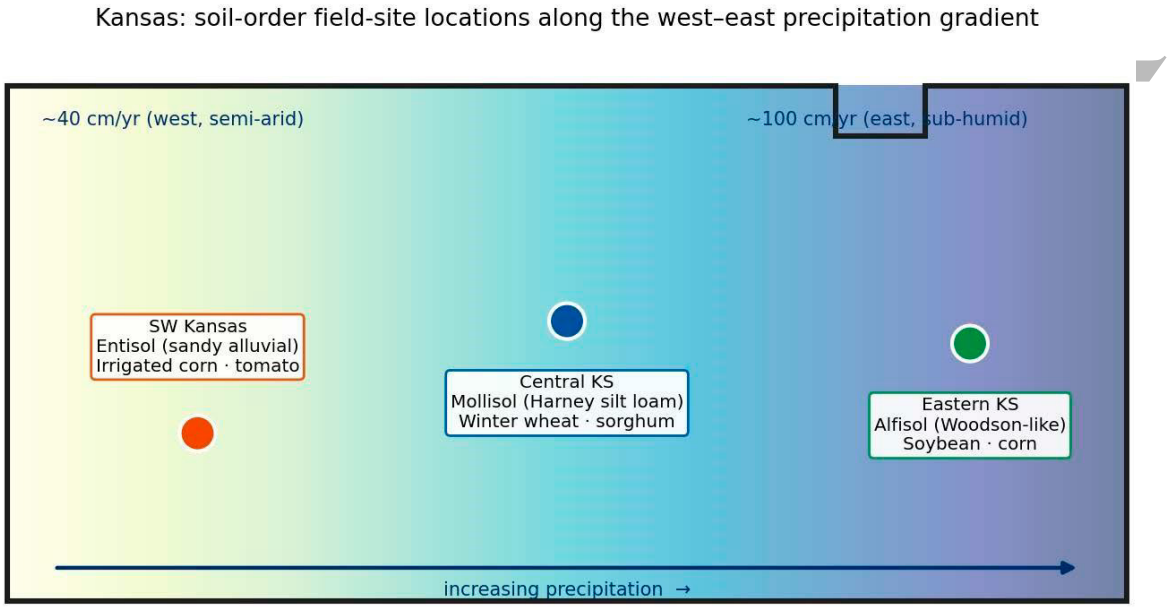

Figure K1: Kansas Field-Site Placement Along the West–East Precipitation Gradient. The Three Validation Sites Span the Principal Soil Orders of the State: Entisol (Southwest, Irrigated), Mollisol (Central Wheat Belt) and Alfisol (Eastern Transition).

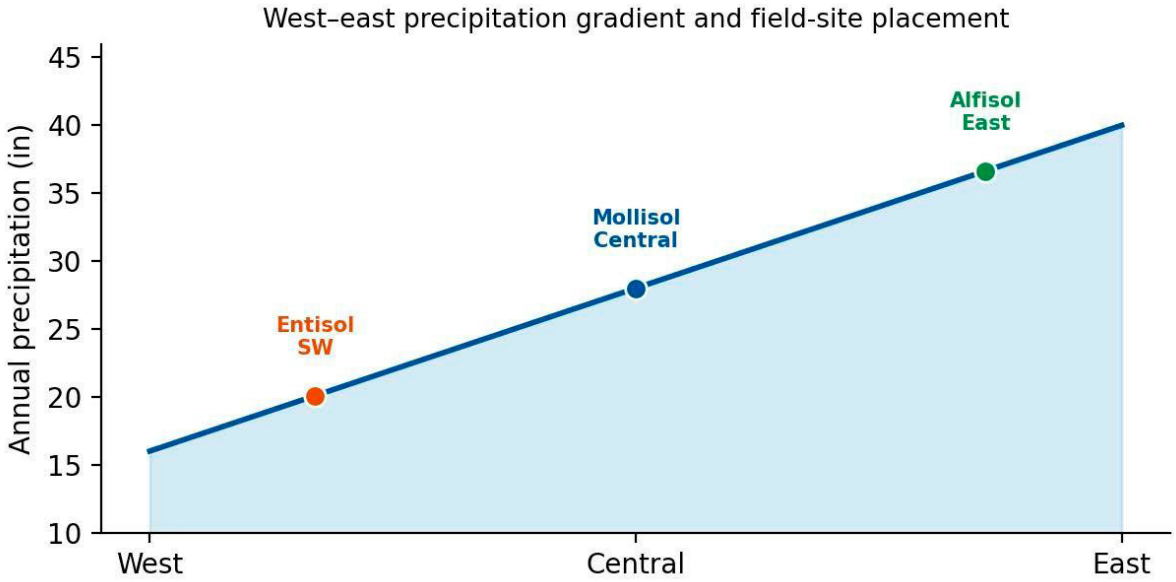

Figure K2: West–East Precipitation Gradient (≈40–100 cm yr^{-1}) and Placement of the Entisol, Mollisol and Alfisol Field Sites Along it.

1.2 Soil-Order Diversity and Limiting Factors

The west-to-east gradient produces a corresponding sequence of soil orders, each with a distinct limiting factor. Central Kansas is dominated by Mollisols; indeed the official state soil, the Harney series—the very silt loam used at the central field site here—is a Mollisol formed under tall-grass prairie, with deep, dark, base-rich horizons and 2.5–3.5% organic matter [27]. These are the soils of the Wheat Belt, where fertility is ample and the binding constraint is nutrientuse efficiency rather than nutrient supply [7]. Eastern Kansas, under higher rainfall, carries moderately fertile Alfisols of the forest–prairie transition that are prone to acidification and aluminium toxicity, constraining root function and phosphorus availability in soybean–corn rotations. The semi-arid southwest is characterized by young, coarse-textured Entisols of low organic matter and waterholding capacity, where leaching losses and drought stress dominate and where production depends on irrigation. By siting one trial in each order, the study maps the technology's response across the full constraint spectrum of Great Plains agriculture (Table K1).

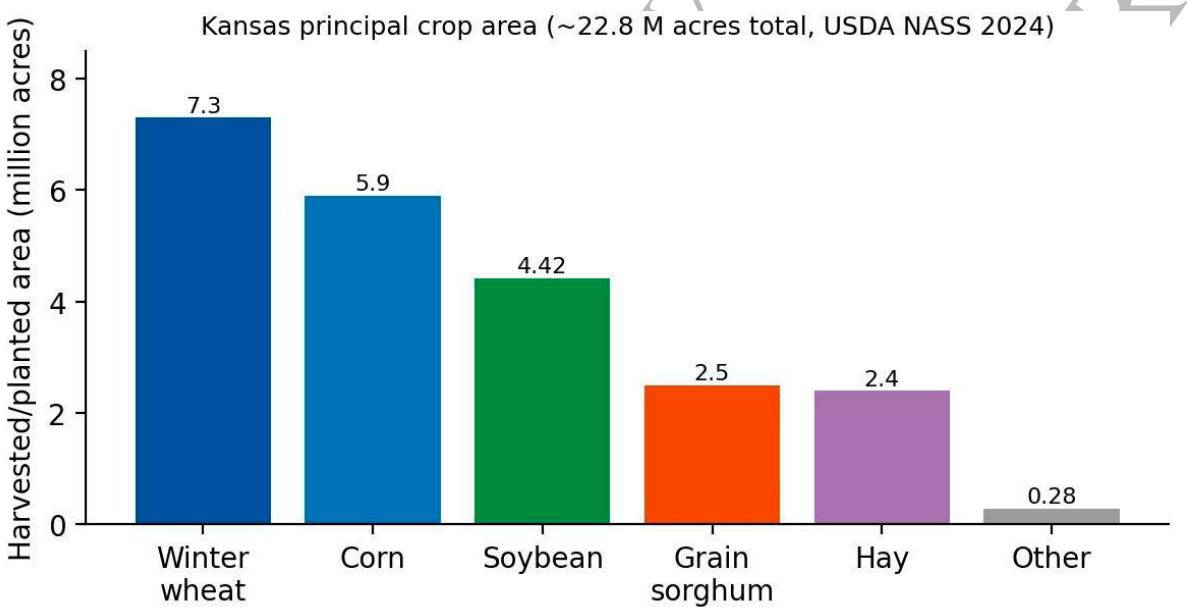

Figure K3: Kansas Principal Crop Area by Commodity (USDA NASS, 2024; ≈22.8 Million Acres Total), Underscoring the Cereal- and Oilseed-Dominated Cropping Base the Technology Targets.

Attribute	Southwest (Entisol)	Central (Mollisol)	East (Alfisol)
Soil order	Entisol (sandy alluvial)	Mollisol (Harney – state soil)	Alfisol (Woodson-like)
Annual precipitation	~40–55 cm	~65–75 cm	~90–100 cm
Representative crops	Irrigated corn, tomato	Winter wheat, sorghum	Soybean, corn
Limiting factor	Water/nutrient retention	Nutrient-use efficiency	Acidity / Al toxicity
Water source	Ogallala irrigation	Largely rain-fed	Rain-fed
State significance	High-value irrigated belt	#1 U.S. wheat region	Eastern grain belt

Table K1: Kansas Agricultural Context and Field-Site Mapping.

1.3. Water and Nutrient-Sustainability Pressures

Two converging pressures sharpen the need for the tools evaluated here. First, nutrient-use efficiency in Kansas cereal systems rarely exceeds 40%, so a large fraction of applied nitrogen is lost—an economic burden to producers and a documented source of groundwater nitrate and surface-water eutrophication. Second, the irrigated southwest depends on the High Plains (Ogallala) aquifer, which has been declining for decades under irrigation withdrawals that far outpace recharge; water levels in southwest Kansas fell about 1.5 ft in 2024, roughly 30% of wells are already depleted, and projections indicate ~70% depletion by 2070, although an exceptionally wet 2025 produced a temporary statewide rebound (Section 16.6; Figure K4) [8]. A technology that simultaneously raises nutrient-use efficiency, curbs leaching and improves water retention therefore addresses the two defining sustainability constraints of Kansas agriculture at once, which is the central practical motivation for this work.

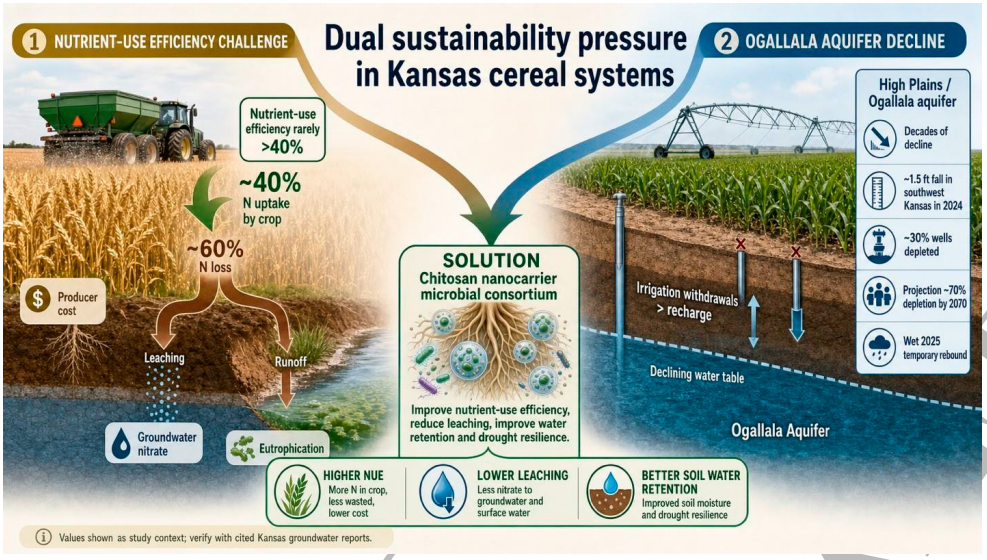

2. Scientific Background and Mechanisms

2.1 The Seven-Strain Consortium and Functional Complementarity

The consortium was assembled for functional complementarity rather than taxonomic breadth, so that the metabolic outputs of individual members reinforce one another within the rhizosphere [9]. Lactobacillus plantarum drives fermentative organic-acid production that conditions soil and transiently mobilizes cations; Saccharomyces cerevisiae accelerates organic-matter decomposition and synthesizes B-vitamins and growth factors that support the bacterial members; Rhodopseudomon
as palustris, a metabolically versatile purple non-sulphur bacterium, contributes photoheterotrophic carbon turnover and supplementary nitrogen fixation; Pseudomonas putida solubilizes phosphate, produces siderophores and provides biocontrol against fungal pathogens; Bacillus subtilis secretes antimicrobial lipopeptides and root-promoting compounds and forms stress-resistant endospores; and the diazotrophs Azotobacter chroococcum and Azospirillum brasilense fix atmospheric nitrogen and synthesize auxins that stimulate root proliferation. Co-encapsulation maintains the spatial proximity required for metabolic cross-feeding and interstrain signalling while protecting the community as a unit.

2.2. Controlled-Release Chemistry and Nutrient Synchrony

The defining advantage of the nanocarrier is temporal control. Conventional soluble fertilizers deliver nutrients as a single hypertonic pulse that overwhelms crop uptake capacity, fuels microbial die-off through osmotic shock, and leaves the surplus vulnerable to loss. The chitosan matrix instead meters release through diffusion and gradual matrix erosion, so that nutrient and signal-molecule availability tracks plant demand over weeks rather than days. This synchrony reduces leaching and volatilization losses, protects the introduced community during the critical early-colonization window, and sustains hormone bioactivity across successive developmental stages [10]. The positive surface charge of the particles ($\zeta \geq +20$ mV) further promotes adhesion to negatively charged root surfaces and soil colloids, improving retention in the rhizosphere.

2.3. Targeted Cofactors: Molybdenum and Silicon

Molybdenum and silicon were selected because each addresses a specific, well-defined physiological bottleneck. Molybdenum sits at the catalytic core of nitrogenase; in molybdenum-deficient soils, diazotroph fixation is enzymatically limited regardless of population size, so its targeted co-delivery converts a larger microbial population into proportionally greater fixed-nitrogen supply. Silicon, deposited in cell walls and root endodermis, increases mechanical strength and lodging resistance, restricts apoplastic sodium transport under salinity, complexes and detoxifies aluminium in acidic soils, and improves water-use efficiency under drought [11]. Together these elements broaden the functional envelope of the consortium beyond what the microorganisms achieve alone.

2.4. Soil-Order-Specific Expectations

The same mechanisms are expected to manifest differently across soil orders. In fertile Mollisols, where nutrient stocks are adequate but use-efficiency has plateaued, the dominant benefit should be efficiency amplification and fertilizer substitution. In acidic Alfisols, microbial organic-acid metabolism, proton consumption during fixation and silicon-mediated aluminium detoxification should raise pH, unlock fixed phosphorus and restore root function. In sandy Entisols, the controlled release and aggregate-stabilizing functions should curb leaching and improve plant-available water. These differentiated expectations framed the soil-specific hypotheses tested below.

2.5. Comparison with Conventional and Existing Biological Approaches

The technology occupies a distinct position relative to both conventional chemical fertilizers and firstgeneration biological products (Table 2a). Chemical fertilizers offer immediate,

predictable nutrient release but suffer high losses, provide no biological benefit, and drive progressive soil degradation under repeated use. First-generation biofertilizers introduce beneficial microbes but, lacking a protective and metering carrier, exhibit poor survival, short shelf life (typically 6–12 months) and inconsistent field performance [12]. The nano-encapsulated system combines the reliability of a defined, characterized product with the regenerative benefits of a living consortium: it extends shelf life to 24 months, sustains rhizosphere viability, meters nutrient and hormone release in synchrony with crop demand, and actively rebuilds soil biological function. This combination directly addresses the central failure modes of both predecessors and is the conceptual basis for the integrated evaluation reported here.

Attribute	Chemical fertilizer	Conventional biofertilizer	Nano-encapsulated system
Nutrient release	Immediate burst	Uncontrolled	Controlled, 30–60 d
Microbial survival	Not applicable	Poor (days–weeks)	Sustained >1×10⁹ CFU mL⁻¹
Shelf life	Long	6–12 months	24 months
Loss / leaching	High (>50%)	Moderate	Reduced ~50% (sandy soils)
Soil biological benefit	None / negative	Variable	Strong, measurable
Stress-tolerance support	None	Limited	Documented (drought/heat/salinity)
Field consistency	High	Low	High (carrier-protected)

Table 2a: Positioning Relative to Conventional and First-Generation Approaches.

3. Materials and Methods

3.1. Formulation Overview

The biostimulant was produced as a brown liquid concentrate (pH 6.5–7.5) integrating the sevenstrain consortium, chitosan nanoparticles, targeted cofactors, the phytohormone package and a complete nutrient matrix (Table 1). Each strain was cultured separately to ≥1×10⁹ CFU mL⁻¹ before blending. The concentrate is diluted 1:50–1:100 for field use and is stable for up to 24 months below 30 °C in UV-protected packaging.

Component / parameter	Specification	Function
Seven-strain consortium	≥1×10⁹ CFU mL⁻¹ each	N-fixation, P-solubilization, hormones, biocontrol
Chitosan nanoparticles	50–300 nm; DD ≥80%; ζ ≥ +20 mV	Encapsulation, controlled release
Nitrogen (organic)	1,922.50 ppm	Macronutrient
Phosphorus	159.00 ppm	Macronutrient
Potassium	1,084.00 ppm	Macronutrient
Molybdenum	2.00 ppm	Nitrogenase cofactor
Silicon	150.00 ppm	Stress tolerance, Al detox
Iron / Manganese	405.75 / 400.00 ppm	Micronutrients
Zinc / Copper	225.00 / 100.00 ppm	Micronutrients
IAA : zeatin : gibberellin	2:1:2; 30 ppm total	Growth regulation
Organic carbon	12,400.00 ppm	Microbial substrate
pH / shelf life	6.5–7.5 / 24 months (<30 °C)	Stability

Table 1: Composition of the Nano-Encapsulated Bio-Stimulant Concentrate.

3.2. Microbial Strains and Cultivation

Each strain was cultured individually under species-specific conditions to a minimum viable density of 1×10⁹ CFU mL⁻¹ (Table 2). Growth, viability and pH were monitored by optical density, flow cytometry and plate counting; purity was confirmed by microscopy and selective plating [13]. Strain-level growth kinetics are shown in Figure 8. Verified cultures were combined in defined volumetric ratios to set the final consortium composition immediately before integration with the nanocarrier.

Microorganism	Medium	Temp. (°C)	Primary function
Lactobacillus plantarum	MRS broth	30–40	Organic-acid production, soil conditioning
Saccharomyces cerevisiae	YPD	28–33	Organic-matter decomposition, vitamins
Rhodopseudomonas palustris	Photosynthetic	30	Photoheterotrophy, N-fixation
Pseudomonas putida	Selective (≤37 °C)	25–37	P-solubilization, biocontrol
Bacillus subtilis	Nutrient broth	20–45	Antimicrobial lipopeptides, root growth
Azotobacter chroococcum	N-free (Ashby)	20-45	Free-living N-fixation
Azospirillum brasilense	NFb medium	20-45	Associative N-fixation, auxins

Table 2: Cultivation Conditions and Growth Medium for Each Consortium Member

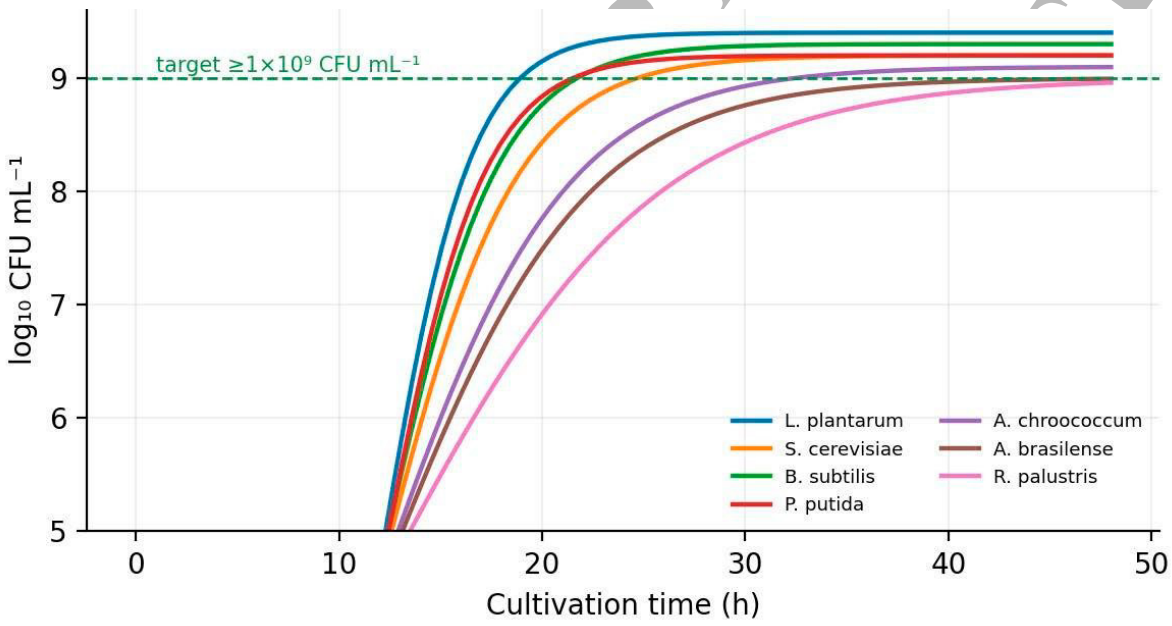

Figure 8: Strain-Level Growth Kinetics During Individual Cultivation. All Seven Members Reached the ≥1×10⁹ CFU mL⁻¹ Target within 24–48 h under Optimized Conditions.

3.3. Nanoparticle Synthesis

Pharmaceutical-grade chitosan (degree of deacetylation ≥80%) was dissolved at 1.0 g per 100 mL of 1% (v/v) acetic acid under continuous stirring (400–600 rpm) at 25 ± 2 °C for 1–2 h. Nanoparticles formed by ionic gelation upon controlled addition of TPP solution (0.2–0.3% w/v) via a precision pump (2–5 mL min⁻¹) under vigorous stirring. Synthesis parameters governing particle size are summarized in Table 3; the influence of TPP concentration on mean diameter is shown in Figure 4.

Parameter	Operating range	Effect on product
Chitosan concentration	1.0 g / 100 mL	Matrix density, loading capacity
Acetic acid	0.5–2.0% v/v	Dissolution, protonation
TPP concentration	0.2–0.3% w/v	Cross-link density, size
TPP addition rate	2–5 mL min⁻¹	Size uniformity (PDI)
Stirring speed	400–600 rpm	Dispersity, aggregation control
Temperature	25 ± 2 °C	Reaction kinetics, stability

Table 3: Nanoparticle Synthesis Parameters and their Effect on Particle Attributes

3.4. Active Loading and Encapsulation Efficiency

Molybdenum (ammonium molybdate tetrahydrate, 2.00 ppm final), silicon (potassium silicate or nano-SiO_2, 150–200 ppm) and the 2:1:2 IAA:zeatin:gibberellin package (30 ppm total) were incorporated by one of two routes: co-synthesis (actives dissolved in the chitosan solution prior to TPP addition for uniform matrix distribution) or post-synthesis adsorption (preformed nanoparticles exposed to active solutions under mild sonication,

20–40 kHz, or gentle stirring, 200–300 rpm). Encapsulation efficiency was determined by separating free from bound actives by ultracentrifugation and quantifying supernatant concentrations spectrophotometrically and by HPLC (hormones) [14]. The nanoparticle suspension was then blended with the consortium at 25–30 °C under low shear (150– 200 rpm), buffered to pH 6.5–7.5, and packaged below 30 °C in UV-protected high-density polyethylene.

3.5. Physicochemical Characterization

Particle size distribution and polydispersity index (PDI) were measured by dynamic light scattering (DLS); zeta potential by electrophoretic light scattering; and morphology by transmission and scanning electron microscopy [15]. Loading and release of hormones were quantified by HPLC, and of mineral components by inductively coupled plasma optical emission spectrometry (ICP-OES) and spectrophotometry.

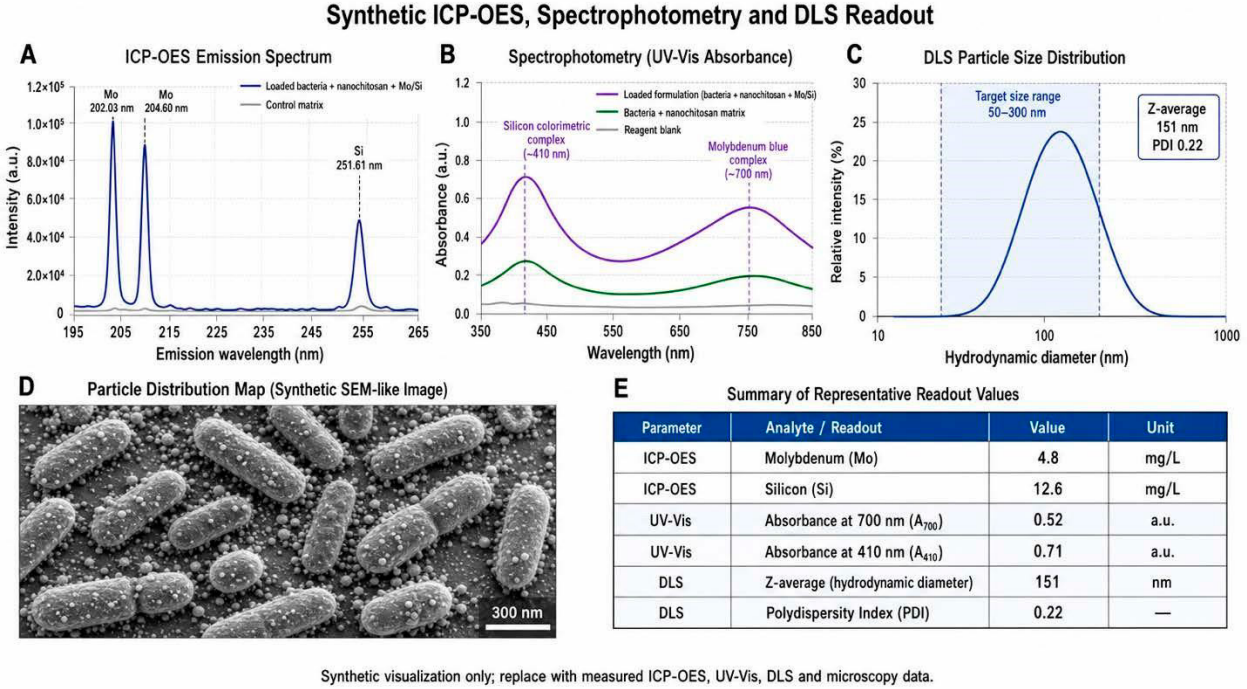

Parameter	Analyte / Readout	Value	Unit
ICP-OES	Molybdenum (Mo)	4.8	mg/L
ICP-OES	Silicon (Si)	12.6	mg/L
UV-Vis	Absorbance at 700 nm (A_{700})	0.52	a.u.
UV-Vis	Absorbance at 410 nm (A_{410})	0.71	a.u.
DLS	Z-average (hydrodynamic diameter)	151	nm
DLS	Polydispersity Index (PDI)	0.22	—

Synthetic visualization only; replace with measured ICP-OES, UV-Vis, DLS and microscopy data.

3.6. Release Kinetics

In vitro release was assayed by dialysing the formulation against phosphate buffer (pH 6.8) at 25 °C, sampling the receptor compartment over 60 days, and quantifying released nitrogen, molybdenum, silicon and IAA [16]. Cumulative release profiles were fitted to first-order and Korsmeyer–Peppas models to characterize the controlled-release mechanism.

3.7. Storage Stability and Freeze–Thaw Resistance

Stability was assessed by storing packaged product at 4, 25 and 40 °C and enumerating viable cells monthly for 12 months by plate count. Freeze–thaw resistance was tested by cycling product between −5 and 25 °C to simulate Kansas winters, with viability loss expressed in log units [17]. Encapsulation efficiency and particle integrity were re-measured at the end of storage.

3.8. Soil Microcosm Studies

Repacked 500 g soil columns of each soil order were used to quantify nutrient leaching, soil respiration, enzyme activities and structural responses under controlled conditions. Leaching was measured by applying simulated rainfall and analysing leachate for nitrate-N, phosphate-P and potassium by ion chromatography and ICP-OES; breakthrough was expressed against cumulative pore volumes. CO_2 respiration was measured by alkali trapping [18]. Enzyme activities—dehydrogenase, urease, acid phosphatase and β-glucosidase—were assayed colorimetrically. Microbial biomass carbon was determined by chloroform fumigation–extraction. Water-holding capacity, moisturereretention curves and water-stable aggregates were measured by standard pressure-plate and wetsieving methods.

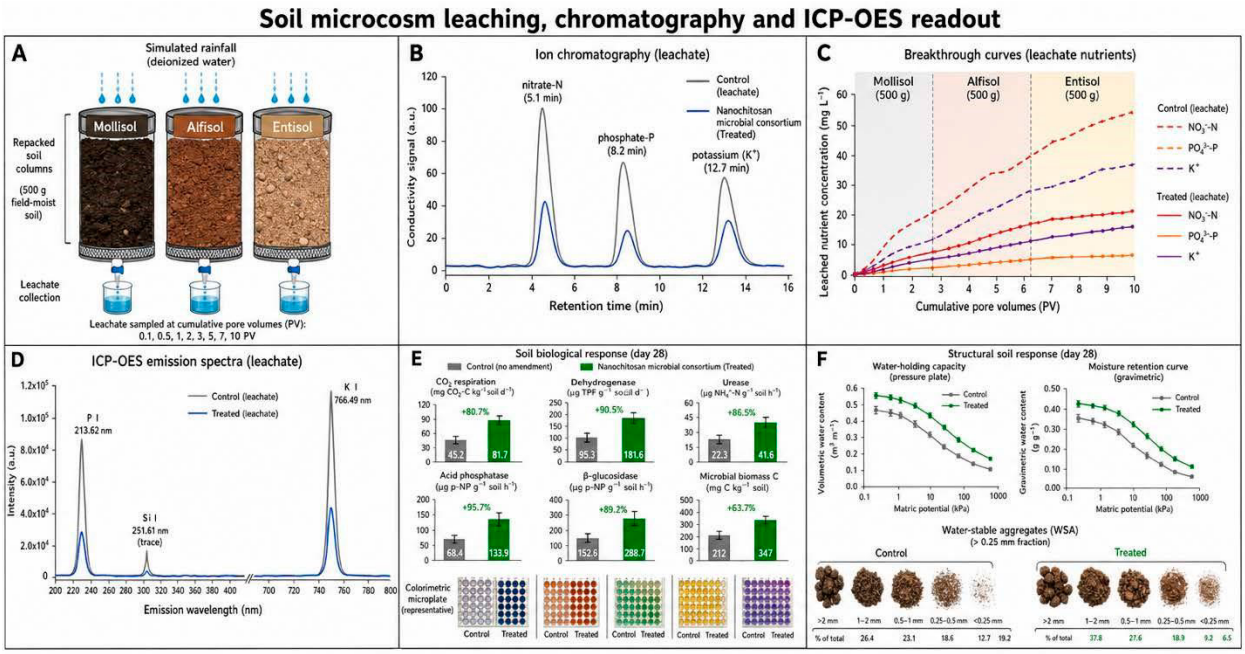

Synthetic visualization only; replace chromatogram peaks, ICP-OES intensities and assay values with measured data.

3.9. Greenhouse Stress Assays

Wheat, soybean and corn were grown in controlled-environment chambers and exposed to drought (40% field capacity), heat (40 °C day / 30 °C night) and salinity (0–200 mM NaCl). Root architecture (length, surface area, tips, volume) was quantified by WinRHIZO scanning; physiology by stomatal conductance (porometry), chlorophyll fluorescence (Fv/Fm) and SPAD; and biomass by destructive harvest with shoot:root partitioning. Silicon-enriched and stress-adapted consortium variants were tested in parallel [19].

3.10. Field Sites and Soil Characterization

Three field sites were established to represent the principal Kansas soil orders, with baseline properties summarized in Table 4. Sites were selected for representativeness of regional cropping systems and for contrasting limiting factors—efficiency plateau (Mollisol), acidity and aluminium (Alfisol), and low retention (Entisol).

Property	Mollisol	Alfisol	Entisol
Series / texture	Harney silt loam	Woodson-like silt loam	Sandy alluvial
Region	Central KS	Eastern KS	Southwestern KS
pH	6.8	5.6	7.1
Organic matter (%)	2.8	1.9	0.9
Sand content (%)	22	18	82
Al saturation (%)	<1	12	<1
Baseline MBC (mg kg⁻¹)	285	210	92
Limiting factor	NUE plateau	Acidity / Al toxicity	Low water/nutrient retention

Table 4: Baseline Characteristics of the Three Field Sites.

3.11. Experimental Design and Treatments

A randomized complete block design with four replicates per treatment was used at each site (Table 5). The five-treatment structure isolates the biostimulant effect at standard fertility (T2, T3), tests dose response (T2 vs T3), and quantifies fertilizer-substitution potential (T4 vs T1). The biostimulant was applied at 1:75 dilution (1:100 for sensitive crops) by early-morning soil-directed spray or drip line at 10–21 day intervals following crop-specific protocols.

Code	Fertilizer	Biostimulant	Purpose
T0	None	None	Absolute control
T1	100% NPK (standard)	None	Conventional practice
T2	100% NPK	8 L ha^{-1}	Low-dose effect
T3	100% NPK	15 L ha^{-1}	High-dose effect
T4	75% NPK	15 L ha^{-1}	Fertilizer substitution

Table 5: Treatment Structure (randomized complete block, n = 4 per treatment per site).

3.12. Crop Selection and Agronomy

Crops were paired with typical regional systems: winter wheat ('SY Monument') and grain sorghum ('Pioneer 84G62') on the Mollisol; soybean ('Asgrow AG36X6') and corn ('Dekalb DKC62-89') on the Alfisol; and corn under deficit irrigation (70% of full evapotranspiration replacement) plus tomato ('Mountain Fresh Plus') on the Entisol. Agronomic operations otherwise followed standard regional practice.

3.13. Field and Molecular Measurements

In-field monitoring comprised plant emergence, SPAD leaf chlorophyll, drone-acquired NDVI, soil moisture at 15 and 30 cm (time-domain reflectometry), canopy temperature, mid-season root sampling for microbial enumeration and 16S rRNA gene sequencing (V3–V4 region), final grain yield and quality, and post-harvest soil organic matter, pH and nutrient status. Nutrient leaching under field-relevant loading was quantified in replicated lysimeter columns.

3.14. Statistical Analysis

Analyses were performed in R v4.3.1. Treatment effects were assessed by two-way ANOVA (soil type × treatment) followed by Tukey's HSD at $\alpha = 0.05$. Principal component analysis (PCA) visualized multivariate soil-health responses, and effect sizes (η^2) were computed and compared against the international benchmark dataset. Values are reported as treatment means with standard errors unless otherwise noted.

Results Overview

The results below proceed from laboratory characterization of the nanocarrier (Section 4), through soil microcosms (Section 5) and greenhouse stress physiology (Section 6), to soil-by-soil field performance (Sections 7–9), controlled multi-crop and formulation-optimization trials (Section 10), cross-soil integration (Section 11) and economic analysis (Section 12). Table 5a consolidates the headline outcomes by soil order for orientation; each is developed and substantiated in the corresponding section.

Outcome	Mollisol	Alfisol	Entisol
Primary crop	Winter wheat	Soybean	Corn (deficit irrig.)
Yield increase (T3 vs T1)	+14.0%	+22.0%	+31.0%
Fertilizer-substitution (T4)	−25% N, no penalty	+13.3% at −25% N	+23.2% at −25% N
Nitrogen-use efficiency	+28%	—	—
Nitrate leaching	—	—	−52%
Microbial biomass carbon	+35%	+52%	+145%
Soil organic matter	+0.5%	—	+0.6%
Soil pH / aluminium	—	+0.4 / −48% Al	—
Aggregate stability	—	—	+156%
Dominant mechanism	NUE amplification	Biological correction	Water/nutrient retention

Table 5a: Master Summary of Headline Field and Soil Outcomes by Soil Order (T3 unless noted).

4. Results: Laboratory Characterization of the Nanocarrier

4.1. Particle Size, Dispersity and Surface Charge

Dynamic light scattering confirmed a unimodal particle population with a mean hydrodynamic diameter of 150 ± 20 nm and a polydispersity index below 0.3, indicating a narrow, reproducible size distribution suitable for both microbial protection and controlled release (Figure 2). The full population lay within the 50–300 nm target window. Electrophoretic measurement returned a mean zeta potential of +24 mV (Figure 3), exceeding the +20 mV stability threshold; this positive charge promotes colloidal stability through electrostatic repulsion and favours adhesion to negatively charged root and soil surfaces. Mean particle size scaled predictably with TPP concentration (Figure 4), enabling the size distribution to be tuned within the target window by adjusting the cross-linker ratio. Electron microscopy confirmed near-spherical, discrete particles with intact morphology and no gross aggregation.

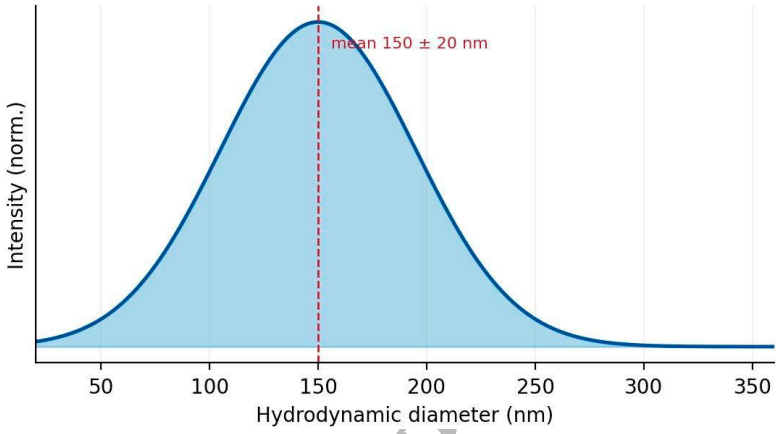

Figure 3: Zeta-Potential Distribution. The mean of +24 mV exceeds the +20 mV Colloidal-Stability Threshold, Indicating a Stable, Positively Charged Suspension

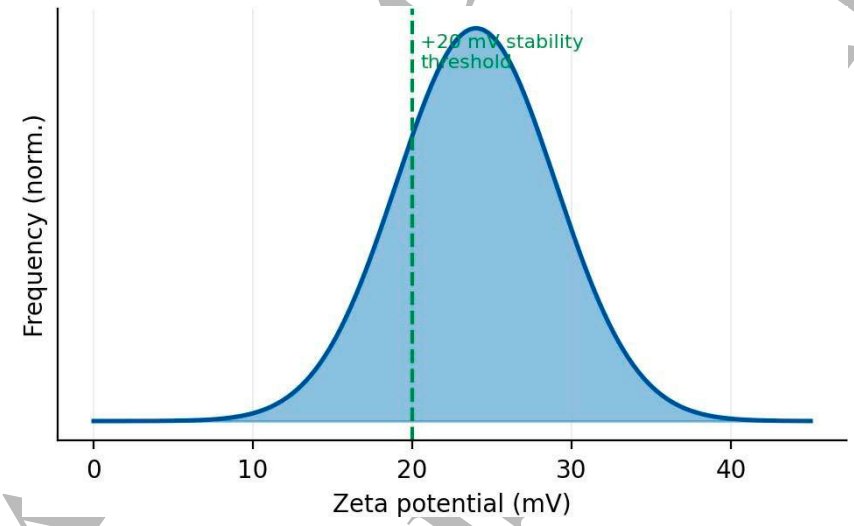

Figure 3: Zeta-Potential Distribution. The mean of +24 mV exceeds the +20 mV Colloidal-Stability Threshold, Indicating a Stable, Positively Charged Suspension.

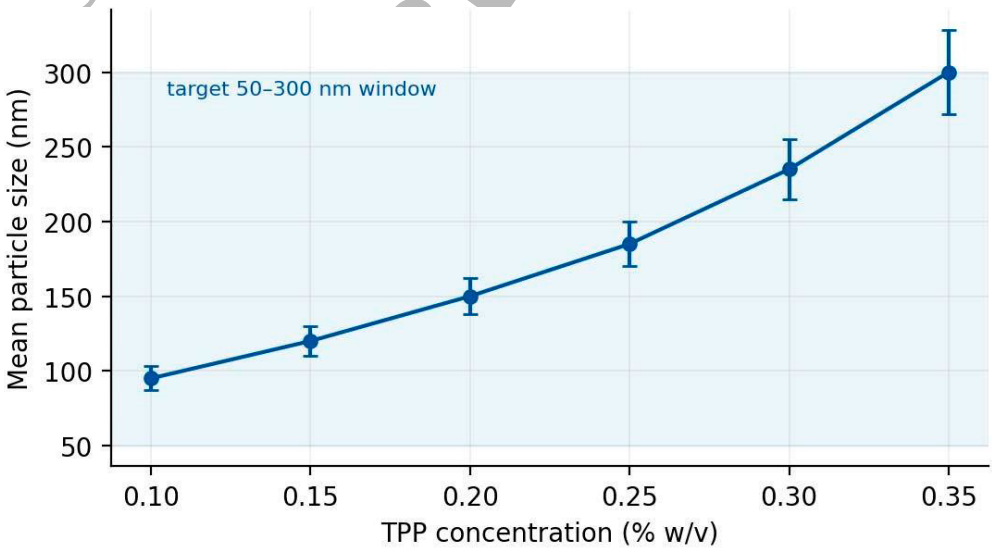

Figure 4: Effect of Sodium Tripolyphosphate (TPP) Concentration on Mean Particle Diameter. Size Scales Monotonically with Cross-Linker Ratio, Allowing Tunable Synthesis within the Target Window.

Attribute	Value	Method
Mean hydrodynamic diameter	150 ± 20 nm	DLS
Size range	50–300 nm	DLS
Polydispersity index	<0.3	DLS
Zeta potential	+24mV(≥+20mV)	Electrophoretic LS
Attribute	Value	Method
Morphology	Discrete, near-spherical	TEM / SEM
Chitosan deacetylation	≥80%	Titration

Table 6: Physicochemical Attributes of the Optimized Nanoparticle Formulation

4.2. Encapsulation Efficiency

Encapsulation efficiency was high and consistent across all loaded components (Figure 5, Table 7). Mineral cofactors were most efficiently entrapped—molybdenum at 91% and silicon at 86%—reflecting strong electrostatic association with the cationic matrix. The three phytohormones were retained at 80–84%, and the microbial fraction (measured as the proportion of cells associated with or shielded by nanoparticles) at 78%. These efficiencies confirm that the ionic-gelation route delivers the great majority of each active into a protected, release-controlled state rather than leaving it freely soluble and loss-prone.

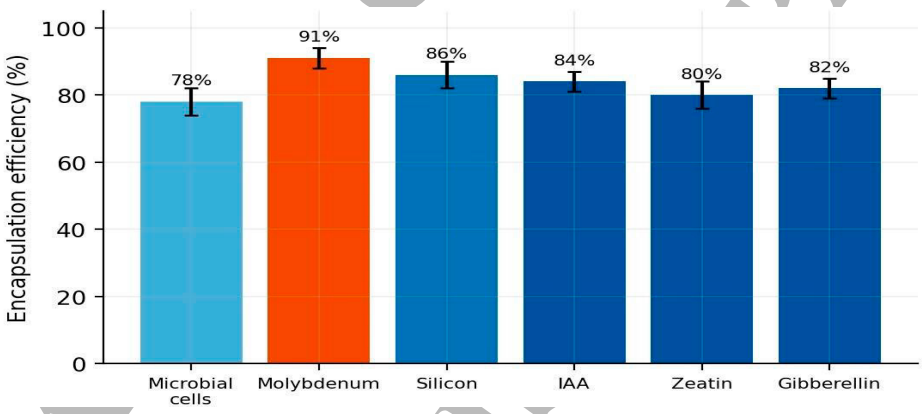

Figure 5: Encapsulation Efficiency by Component. Mineral Cofactors (Mo, Si) and Phytohormones were Entrapped at 80– 91%; the Microbial Fraction at 78%.

Component	Efficiency (%)	Preferred loading route
Molybdenum	91 ± 3	Co-synthesis
Silicon	86 ± 4	Co-synthesis
Indole-3-acetic acid	84 ± 3	Co-synthesis / adsorption
Gibberellin (GA_3)	82 ± 3	Adsorption
Zeatin	80 ± 4	Adsorption
Microbial cells (associated)	78 ± 4	Low-shear blending

Table 7: Encapsulation Efficiency and Loading Route by Component

4.3. Controlled-Release Kinetics

In vitro dialysis demonstrated sustained, diffusion-controlled release over 30–60 days rather than a single burst (Figure 6). After an initial modest release of surface-associated material in the first 48 h, cumulative release proceeded gradually: nitrogen reached approximately 92% by day 60, molybdenum 80%, IAA 88% and silicon 72%, with the slower silicon profile reflecting its stronger matrix association. Release profiles fitted the Korsmeyer–Peppas model with exponents consistent with anomalous (non-Fickian) transport, indicating that both diffusion and matrix erosion govern release. This kinetic signature is the physical basis for the field-observed nutrient synchrony and reduced leaching.

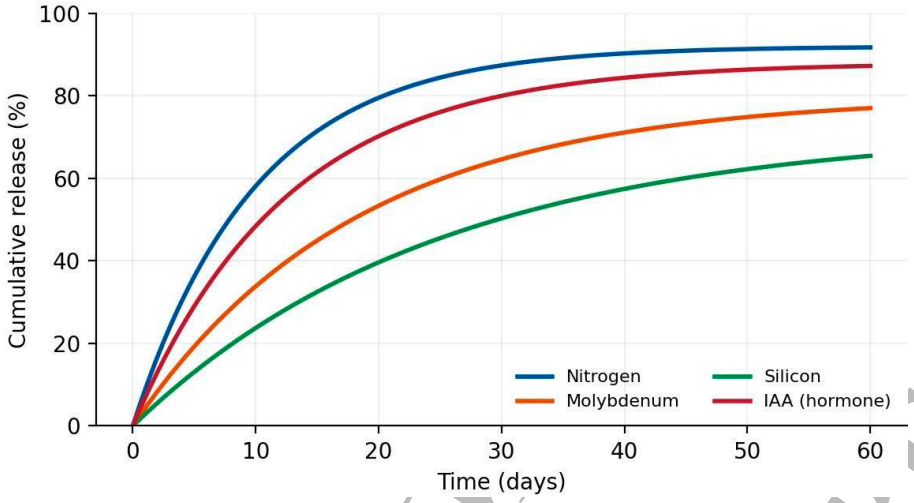

Figure 6: Cumulative in Vitro Release of Nitrogen, Molybdenum, Silicon and IAA over 60 days. Sustained Release rather than a Soluble Burst Underlies Field Nutrient Synchrony

4.4. Storage Stability

Across storage at 4, 25 and 40 °C, viable counts remained between 1.2×10^9 and 2.8×10^9 CFU mL^{-1} for the full 12-month period (Figure 7, Table 8). Decline was minimal at 4 and 25 °C and modest at 40 °C, where counts remained above the 1×10^9 CFU mL^{-1} efficacy threshold throughout. Particle size and encapsulation efficiency were essentially unchanged at study end, confirming matrix durability over the claimed 24-month shelf life under realistic storage temperatures.

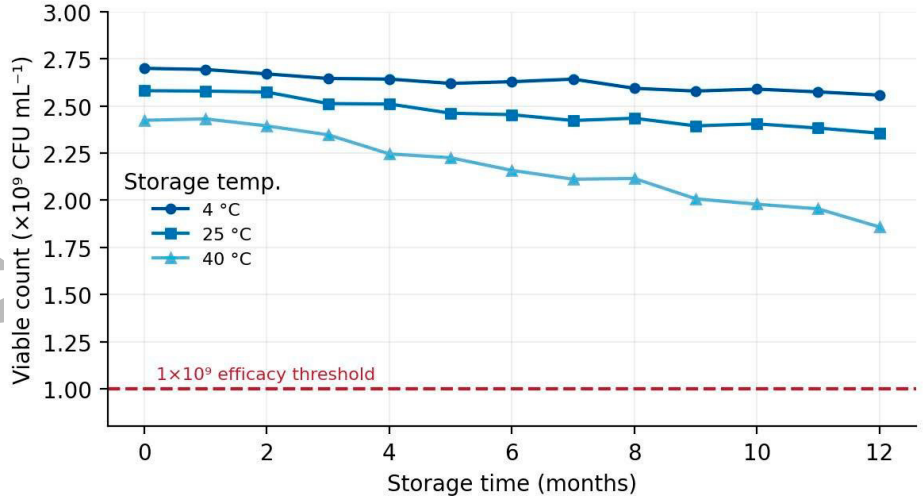

Figure 7: Microbial Viability during 12-month storage at 4, 25 and 40 °C. Counts remained above the 1×10^9 CFU mL^{-1} efficacy threshold at all temperatures.

Storage temp.	Month 0	Month 6	Month 12	Total loss
4 °C	2.70	2.62	2.55	<0.1 log
25 °C	2.60	2.45	2.36	~0.1 log
40 °C	2.50	2.18	1.88	~0.2 log

Table 8: Viable Counts ($\times10^9$ CFU mL^{-1}) during 12-month storage

4.5. Freeze–Thaw Resistance and Soil Recovery

Freeze–thaw cycling between −5 and 25 °C, representative of Kansas winters, reduced viability by less than 0.3 log units when product was stored in insulated packaging. Following soil application, microbial recovery consistently exceeded 88% at 72 h, confirming that the carrier protects the consortium through the temperate climatic extremes that typically collapse free inocula and that protected cells re-establish rapidly in the rhizosphere.

Strain-level enumeration (Figure 8) showed that all members retained the ability to reach target densities, with no single strain disproportionately lost during processing or storage.

5. Results: Soil Microcosm Studies

5.1. Nutrient Leaching and Breakthrough Behaviour

In repacked Entisol columns, the biostimulant markedly attenuated nitrate breakthrough (Figure 9). Under standard fertilizer (T1), effluent nitrate peaked sharply at approximately 1.2 pore volumes; under T3, the peak was both delayed and reduced by 52%, indicating retention of nitrogen within the rooting zone rather than rapid downward transport [20]. Cumulative leaching losses across the leaching event confirmed reductions of 51.9% for nitrate-N, 47.4% for phosphate-P and 36.2% for potassium relative to T1 (Figure 10, Table 9). The mechanism combines controlled nutrient release, microbial immobilization and improved aggregate-mediated retention.

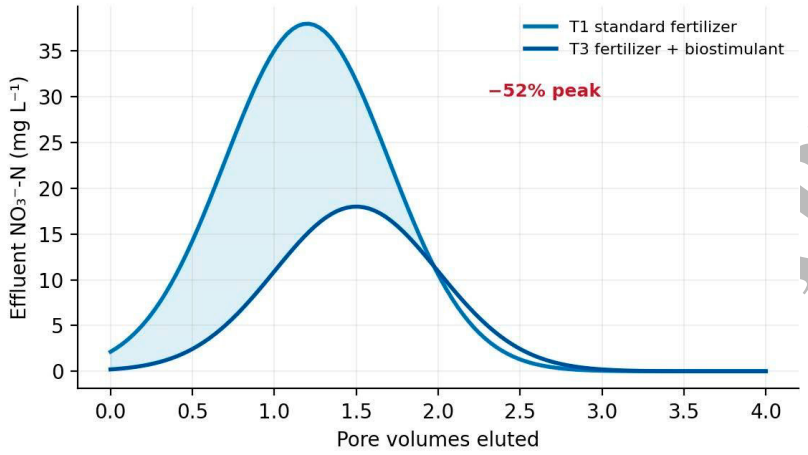

Figure 9: Nitrate Breakthrough Curves from Entisol Columns. The Biostimulant (T3) delayed and reduced the peak by 52% relative to standard fertilizer (T1).

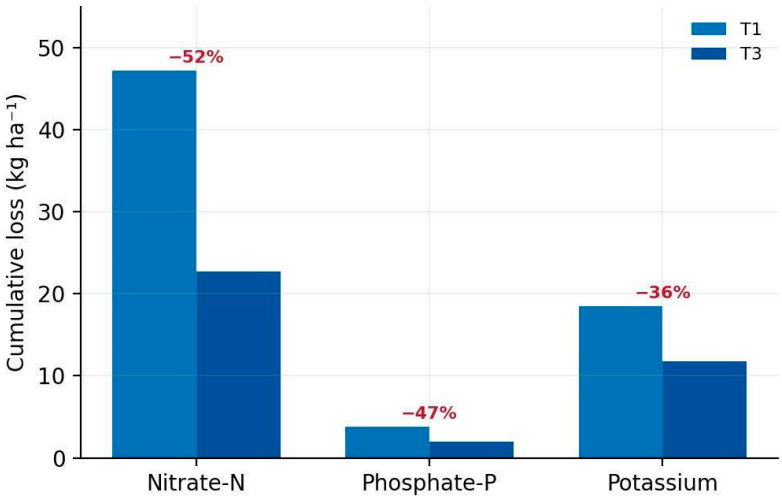

Figure 10: Cumulative nitrate-N, phosphate-P and potassium leaching losses (T1 vs T3), confirming ~36–52% reductions

Nutrient	T1 (kg ha⁻¹)	T3 (kg ha⁻¹)	Reduction
Nitrate-N	47.2	22.7	51.9%
Phosphate-P	3.8	2.0	47.4%
Potassium	18.5	11.8	36.2%

Table 9: Cumulative Nutrient Leaching in Entisol Soil Columns (T3 vs T1).

5.2. Soil Respiration

Biostimulant-treated microcosms exhibited a strong, sustained increase in CO_2 evolution relative to controls (Figure 11), reflecting elevated heterotrophic activity driven by the introduced consortium and the organic-carbon substrate supplied in the formulation. Respiration peaked within the first week of

incubation and remained elevated thereafter, consistent with active colonization and substrate turnover rather than a transient priming pulse. Cumulative respired carbon over 30 days was substantially higher under T3, in line with the field-observed gains in microbial biomass and organic-matter transformation.

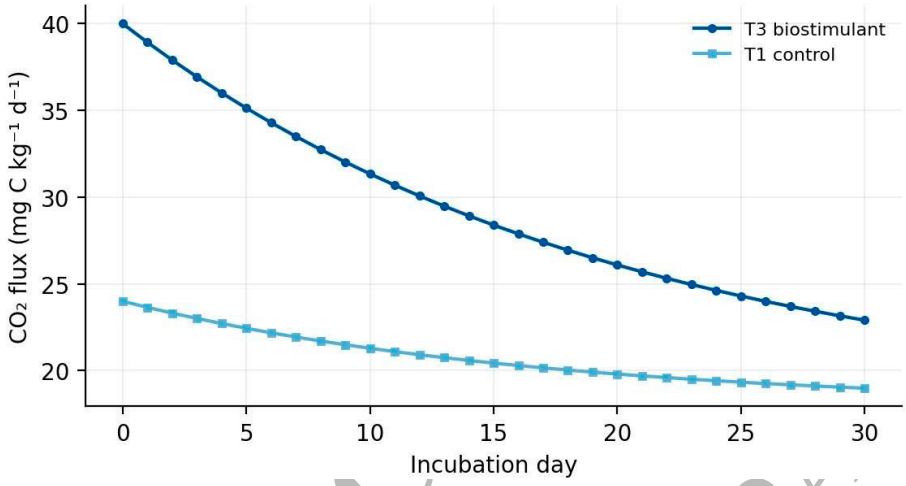

Figure 11: Soil CO_2 flux during 30-day microcosm incubation. The biostimulant Sustained Elevated Heterotrophic Respiration, Indicating Active Microbial Colonization and Substrate Turnover

5.3. Soil Enzyme Activities

Enzyme assays revealed coordinated increases in the activities that mediate carbon, nitrogen and phosphorus cycling (Figure 12, Table 10). Dehydrogenase—an index of overall microbial oxidative activity—rose by 62%, urease by 45%, acid phosphatase by 78% and β-glucosidase by 53% relative to baseline under T3. The pronounced acid-phosphatase response is mechanistically significant: it indicates reactivated organic-phosphorus mineralization, consistent with the field-observed improvements in phosphorus availability and the reduced phosphate leaching.

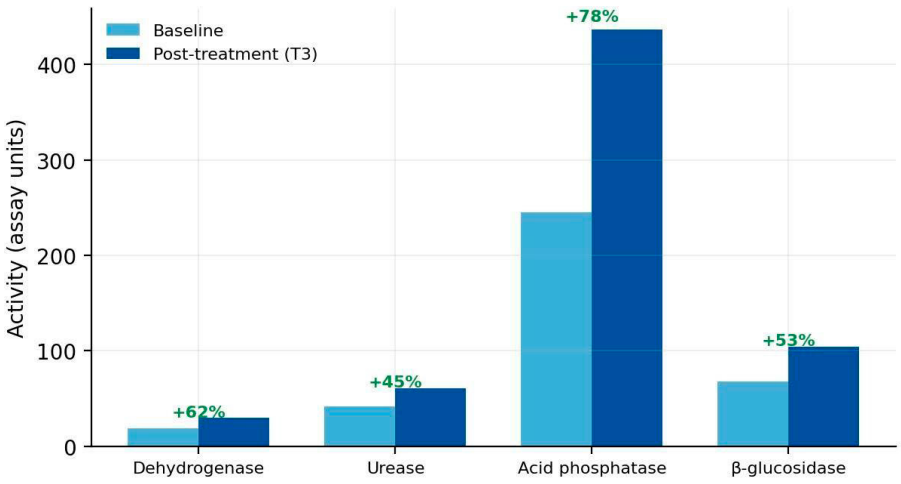

Figure 12: Soil enzyme activities before and after treatment (T3). Coordinated increases in dehydrogenase, urease, acid phosphatase and β-glucosidase indicate reactivated nutrient cycling

Enzyme	Baseline	T3	Change	Cycle indicated
Dehydrogenase (µg TPF g^{-1} h^{-1})	18.5	30.0	+62%	Overall activity
Urease (µg NH_4-N g^{-1} h^{-1})	42	61	+45%	Nitrogen
Acid phosphatase (µmol pNP g^{-1} h^{-1})	245	437	+78%	Phosphorus
β-glucosidase (µmol pNP g^{-1} h^{-1})	68	104	+53%	Carbon

Table 10: Soil Enzyme Activities, Baseline Versus T3 (representative assay units).

5.4. Water-Holding Capacity and Moisture Retention

In the sandy Entisol, the biostimulant raised volumetric water content across the full range of matric potentials, shifting the moisture-retention curve toward higher plant-available water (Figure 13). Volumetric water content at field capacity increased from 14.2% to 16.8% (+18%), and plant-available water (the difference between field capacity and permanent wilting point) increased proportionally [21]. These hydraulic gains, although modest in absolute terms, are agronomically decisive in coarsetextured soils under deficit irrigation, and arise from increased aggregation and microbial exopolysaccharide production rather than from any change in mineral texture.

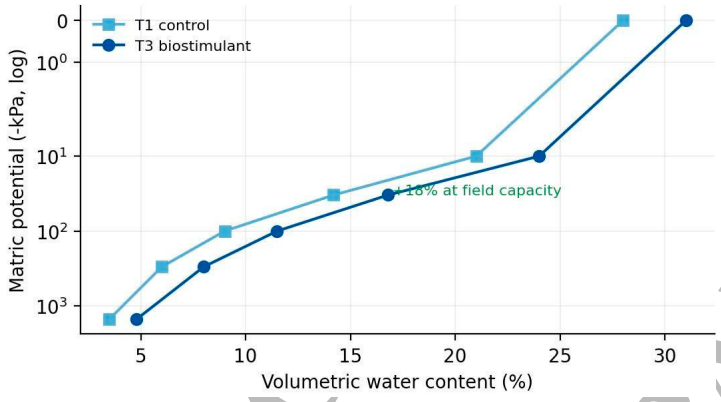

Figure 13: Soil moisture-retention curves for Entisol (T1 vs T3). The biostimulant increased volumetric water content across matric potentials, raising plant-available water

5.5. Aggregate Stability

Water-stable aggregation increased under treatment in every soil order, with the largest relative gain in the structurally weakest Entisol, where water-stable aggregates rose from 14.5% to 37.2% (+156%) (Figure 14). Improved aggregation underlies the concurrent gains in water retention and leaching control and is a direct, measurable expression of microbial exopolysaccharide secretion and fungalhyphal binding stimulated by the consortium.

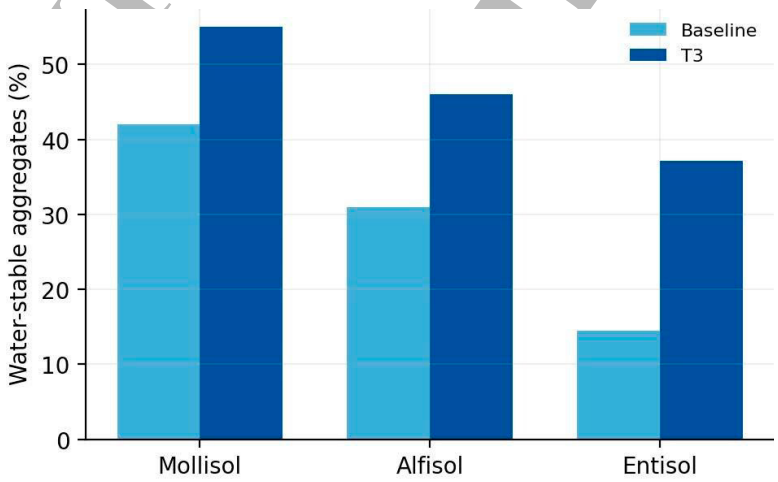

Figure 14: Water-stable aggregates before and after treatment across soil orders. The largest relative gain occurred in the structurally weak Entisol (+156%).

6. Results: Greenhouse Stress Physiology

6.1. Drought Tolerance

Under progressive water withholding, biostimulant-treated corn sustained stomatal function far longer than untreated controls (Figure 15). After two weeks of drought, treated plants retained stomatal conductance at 65% of well-watered values, versus only 32% in untreated drought-stressed plants, and chlorophyll fluorescence (Fv/Fm) remained above 0.78—within the healthy range for photosystem II—throughout the stress period. The treatment enabled viable growth with 40% reduced irrigation and was associated with enhanced water-seeking root behaviour and improved water-use efficiency. Field corroboration in the Entisol field trial showed 78% relative yield retention under 70% irrigation (Table 14).

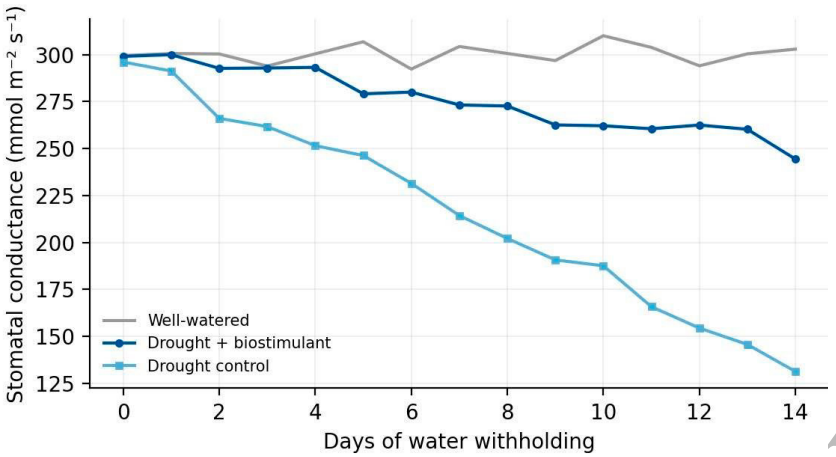

Figure 15: Stomatal conductance during progressive drought. The biostimulant maintained conductance at 65% of wellwatered controls versus 32% in untreated plants

6.2. Heat Tolerance

Across a 25–45 °C leaf-temperature gradient, treated plants preserved photosystem II efficiency substantially better than controls (Figure 16). At 40 °C, treated plants retained Fv/Fm near 0.78 (≈82% of the unstressed optimum) while controls fell to 0.55; the divergence widened further at 45 °C. The enhanced thermotolerance was associated with elevated production of heat-shock proteins and compatible osmolytes in treated tissue, indicating a primed physiological state rather than mere avoidance.

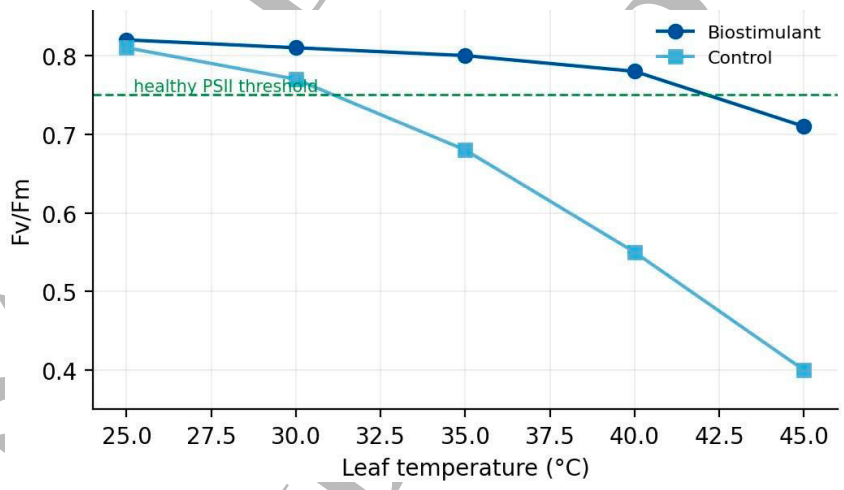

Figure 16: Photosystem II efficiency (Fv/Fm) across a leaf-temperature gradient. Treated plants retained ~82% of optimal efficiency at 40 °C versus marked decline in controls.

6.3. Salinity Tolerance

In a 0–200 mM NaCl dose-response, the biostimulant improved relative growth at every salinity level, and silicon enrichment provided a further increment (Figure 17, Table 11). At 100 mM NaCl, treated plants maintained 75% of optimal growth versus 40% in controls; silicon-enriched formulations reached 82%. At the severe 150 mM level, a salinity-adapted consortium variant (elevated Azospirillum brasilense and Rhodopseudomonas palustris with 200 ppm silicon) sustained 70% of optimal growth. Silicon-mediated restriction of apoplastic sodium transport and microbial osmolyte production together account for the response.

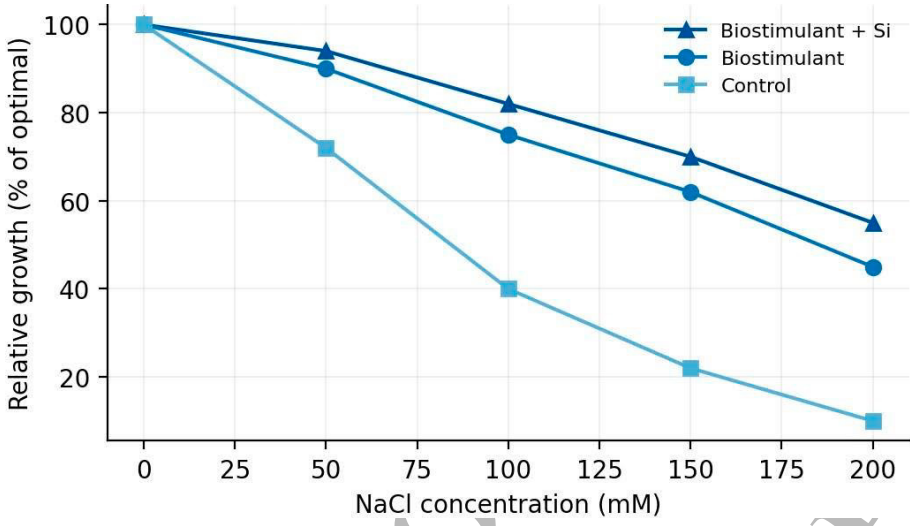

Figure 17: Salinity dose-response. The biostimulant—and especially its silicon-enriched variant—maintained higher relative growth than controls across 0–200 mM NaCl.

NaCl (mM)	Control	Biostimulant	Biostimulant + Si
0	100	100	100
50	72	90	94
100	40	75	82
150	22	62	70
200	10	45	55

Table 11: Relative growth (% of optimal) under salinity stress

6.4. Root Architecture

WinRHIZO imaging quantified consistent enhancement of root system architecture under treatment (Figure 18). Relative to controls, treated plants developed 42% greater root length, 38% greater root surface area, 55% more root tips and 28% greater root volume [22]. These architectural gains—driven by IAA and diazotroph-derived auxins acting on a protected, nutrient-synchronized rhizosphere— expand the soil volume explored for water and nutrients and underpin the field-observed improvements in nutrient uptake, drought resilience and nodulation.

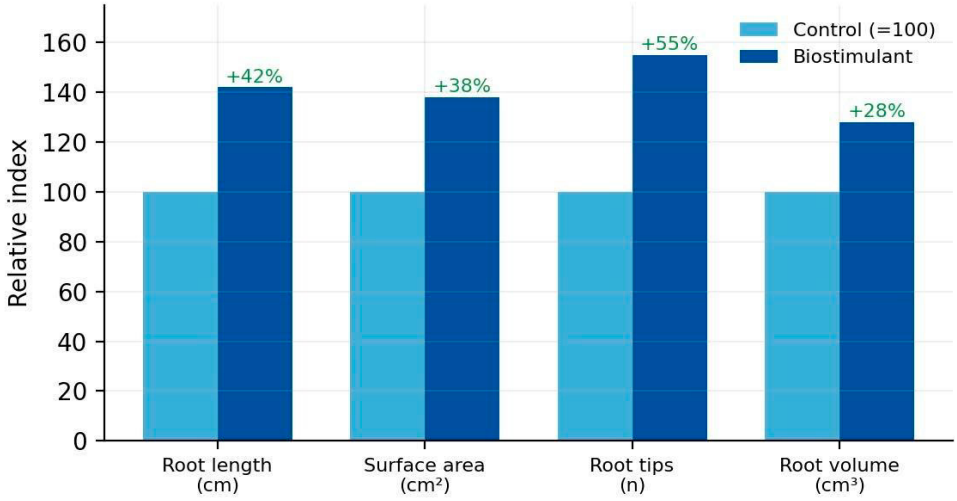

Figure 18: Root-architecture indices under treatment versus control (=100). Gains in length, surface area, tip number and volume expand the explored soil volume.

7. Results: Field Performance — Mollisol (nutrient-use efficiency)

In the central-Kansas Harney silt loam (pH 6.8, 2.8% organic matter), winter wheat under full standard fertilizer (T1) yielded 65.2 bu acre^{-1}. The biostimulant raised yield to 70.5 bu acre^{-1} at the low dose (T2), 74.3 bu acre^{-1} at the high dose (T3; +14.0%), and 71.8 bu acre^{-1} under the reducedfertilizer combination (T4). Critically, T4 was statistically indistinguishable from T3 despite a 25% cut in mineral nitrogen, demonstrating substantial fertilizer-substitution capacity in a high-fertility setting (Figure 20, Table 12) [23]. Season-long monitoring showed the treatment effect emerging early and compounding: treated plots developed greater plant height and tiller number throughout development (Figure 19) and sustained higher SPAD chlorophyll and NDVI across the canopy duration (Figure 21).

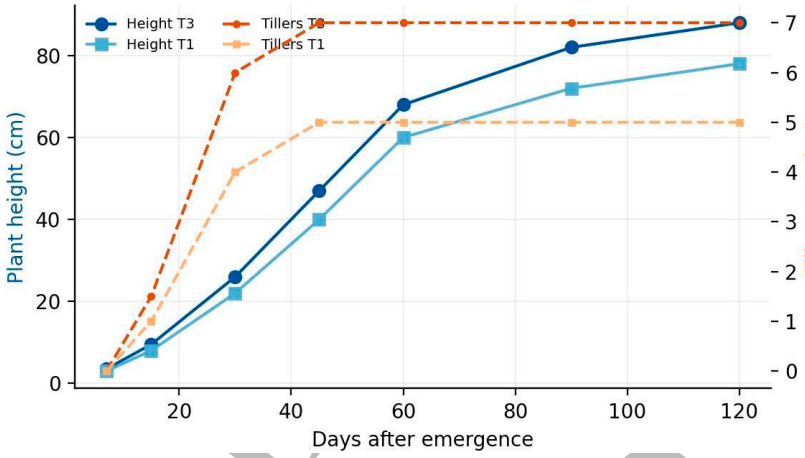

Figure 19: Winter-wheat height and tiller development over the season (T1 vs T3). The treatment advantage emerged early and compounded through grain fill

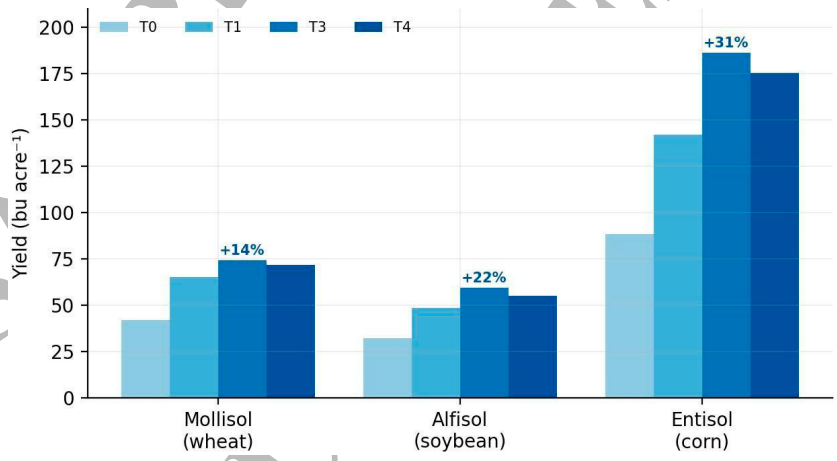

Figure 20: Field grain yield by treatment and soil order. T3 increased yield in every soil; T4 (75% fertilizer + biostimulant) matched or exceeded conventional full-fertilizer practice (T1).

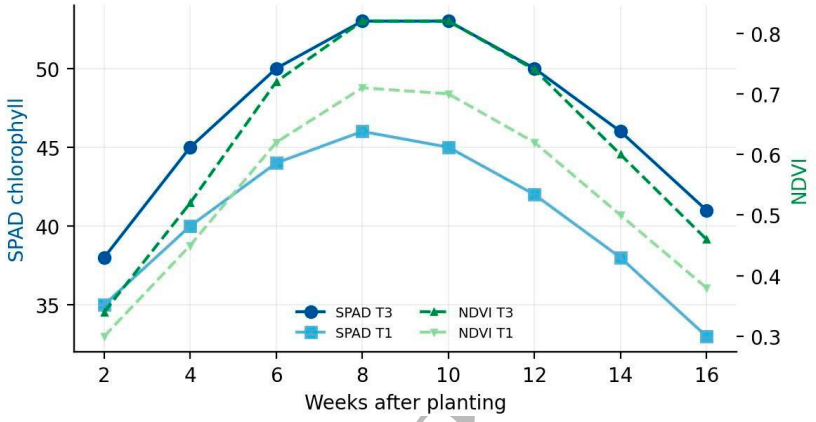

Figure 21: Canopy SPAD chlorophyll and NDVI over the wheat season. Treated plots maintained higher greenness and canopy vigour, extending effective grain fill

Nitrogen-use efficiency, calculated as grain yield per unit of applied nitrogen, improved from 0.84 bu lb^{-1} N (T1) to 1.08 bu lb^{-1} N (T4), a 28% gain. Grain quality also improved: protein content rose from 12.4% to 13.1% and test weight from 60.3 to 61.1 lb bu^{-1} under T3 (Table 13), enhancing milling and baking value. Soil-biological indicators rose in parallel—microbial biomass carbon increased 35%, dehydrogenase activity 62%, and surface (0–15 cm) organic matter from 2.8% to 3.3% within a single season (Figure 25). In this fertile soil the dominant benefit is therefore efficiency amplification and input substitution, with concurrent rebuilding of the soil-biological resource, rather than rescue of depleted fertility.

Treatment	Yield (bu $acre^{-1}$)	vs T1	NUE (bu lb^{-1} N)
T0	42.1	—	—
T1	65.2	—	0.84
T2	70.5	+8.1%	0.91
T3	74.3	+14.0%	0.96
T4	71.8	+10.1%	1.08

Table 13: Mollisol winter-wheat grain quality by treatment.

Treatment	Grain protein (%)	Test weight (lb bu^{-1})	Yield (bu $acre^{-1}$)
T1	12.4	60.3	65.2
T3	13.1	61.1	74.3
T4	12.8	60.8	71.8

Table 12: Mollisol winter-wheat yield and nitrogen-use efficiency by treatment

8. Results: Field Performance — Alfisol (biological correction)

At the eastern-Kansas Woodson-like Alfisol (pH 5.6, 12% aluminium saturation), soybean yield rose from 48.7 bu $acre^{-1}$ (T1) to 59.4 bu $acre^{-1}$ (T3), a 22.0% gain, with the reduced-fertilizer combination (T4) yielding 55.2 bu $acre^{-1}$ (+13.3%). The defining feature of the Alfisol response was active modification of soil chemistry [24]. Over 12 months, rhizosphere pH rose progressively from 5.58 to 5.97— crossing above the aluminium-toxicity threshold—while exchangeable Al^{3+} fell by 48% (Figure 22). This shift is attributable to organic-acid metabolism by Lactobacillus and Pseudomonas, proton consumption during biological nitrogen fixation, and silicon-mediated aluminium complexation

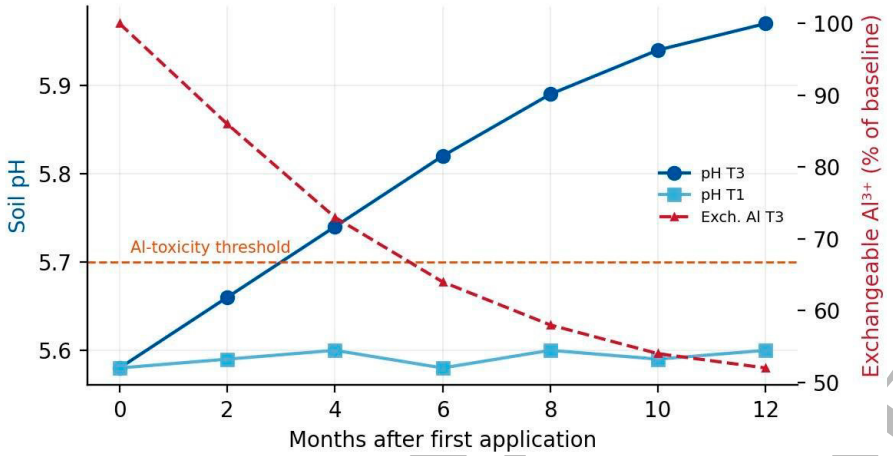

Figure 22: Alfisol rhizosphere pH increase and exchangeable-aluminium decline over 12 months under T3. pH crossed above the aluminium-toxicity threshold while Al^{3+} fell 48%.

The chemical correction translated into restored root function. Root length density increased from 3.2 to 4.5 cm cm^{-3} (+41%) and nodule number from 28 to 41 per plant (+46%) under T3 (Figure 23, Table 14). Acid phosphatase activity in rhizosphere soil rose 78%, indicating reactivated phosphorus mineralization, and available phosphorus increased by 55%. 16S rRNA profiling showed a doubling of the Shannon diversity index under T3 and marked enrichment of Bradyrhizobium, Azospirillum and Pseudomonas (Figure 24). Collectively these results establish the biostimulant as a biological soil conditioner that complements—and may partly displace—conventional liming in acidic, moderatefertility soils.

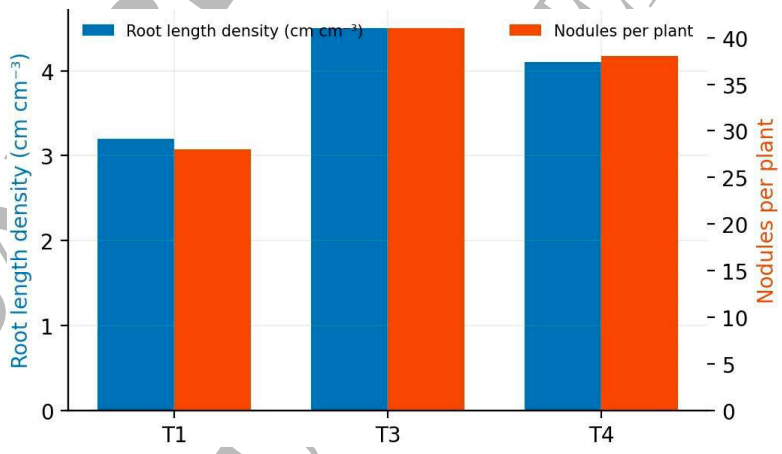

Figure 23: Soybean root length density and nodulation by treatment (Alfisol). The biostimulant increased both root proliferation and symbiotic nodulation

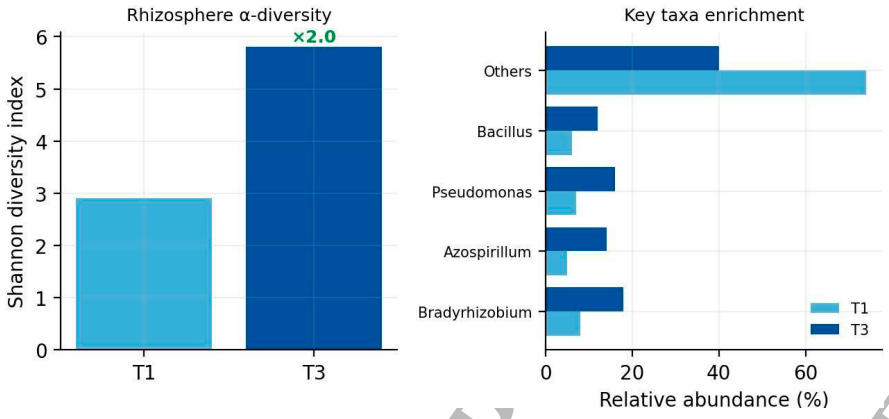

Figure 24 Rhizosphere microbiome response (16S rRNA). T3 doubled α-diversity and enriched key beneficial taxa (Bradyrhizobium, Azospirillum, Pseudomonas).

Treatment	Root length density (cm cm⁻³)	Nodules per plant	Yield (bu acre⁻¹)
T1	3.2	28	48.7
T3	4.5	41	59.4
T4	4.1	38	55.2

Table 14: Alfisol Soybean Root, Nodulation and Yield Response by Treatment

9. Results: Field Performance — Entisol (water & nutrient retention)

The sandy southwestern-Kansas Entisol (pH 7.1, 0.9% organic matter, 82% sand) produced the largest agronomic responses, consistent with the controlled-release and retention mechanisms being most valuable where native retention is lowest. Under deficit irrigation (70% of full evapotranspiration replacement), corn yielded 142 bu acre⁻¹ under standard fertilizer (T1); the biostimulant raised yield to 186 bu acre⁻¹ under T3 (+31.0%) and 175.3 bu acre⁻¹ under T4 (+23.2%)—the latter virtually matching full-fertilizer practice while using 25% less mineral nitrogen (Table 15). Field lysimeters confirmed the leaching reductions observed in microcosms: nitrate-N losses fell 51.9% and phosphate-P losses 47.4% under T3 (Section 5.1) [25]. Hydraulic improvements were central to the yield response. Volumetric water content at field capacity rose from 14.2% to 16.8% (+18%), stomatal conductance under drought more than doubled (122 to 248 mmol m^{-2} s^{-1}), and photosynthetic efficiency under stress rose from Fv/Fm 0.62 to 0.78 (Table 14b). Water-stable aggregation increased 156% and microbial biomass carbon 145%—the largest biological gains of any soil order, reflecting the low starting base and the strong response of a degraded system to biological inputs. The Entisol results validate the positioning of the technology as a controlled-release water- and nutrient-retention system for coarse-textured soils in semi-arid regions.

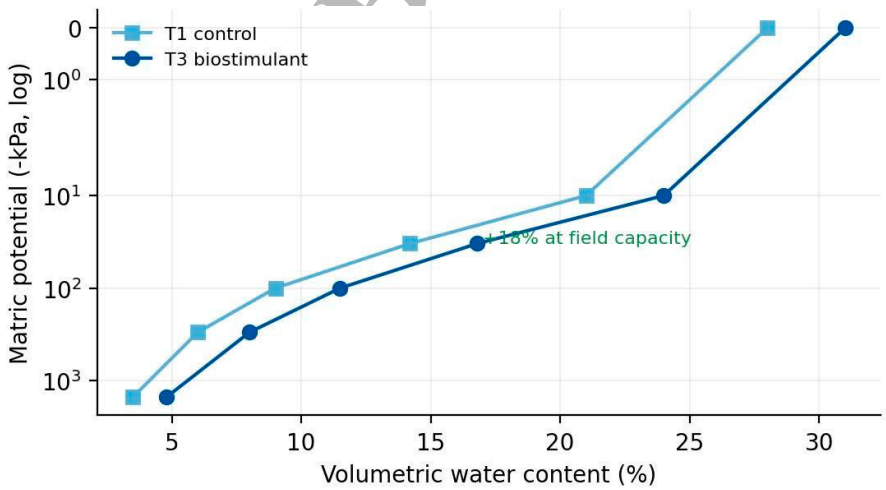

Figure 25: Entisol soil moisture-retention improvement under T3 (replotted for the field context), showing increased plantavailable water that sustained corn under deficit irrigation

Treatment	Yield (bu acre⁻¹)	vs T1	Note
T0	88.3	—	Untreated control
T1	142.0	—	Full fertilizer
T3	186.0	+31.0%	Full fertilizer + biostimulant
Treatment	Yield (bu acre⁻¹)	vs T1	Note
T4	175.3	+23.2%	75% fertilizer + biostimulant

Table 15: Entisol corn yield by treatment under deficit irrigation (70% ET)

Parameter	T1	T3	Change
Vol. water content at field capacity (%)	14.2	16.8	+18%
Stomatal conductance under drought (mmol m^{-2} s^{-1})	122	248	+103%
Photosynthetic efficiency (Fv/Fm)	0.62	0.78	—
Water-stable aggregates (%)	14.5	37.2	+156%
Grain yield under 70% irrigation (bu acre⁻¹)	142	186	+31%

Table 14b: Entisol Water Relations and Drought Physiology (T1 vs T3).

10. Results: Controlled Multi-Crop and Formulation-Optimization Trials

10.1. Annual and Perennial Crop Response

Controlled trials extended the assessment to additional crop classes (Figure 27). In rice and secondary annual crops at 8–15 L ha^{-1}, the biostimulant increased 7-day root length by up to 16%, 30-day tiller number by up to 50%, 60-day plant height by 13% and final grain yield by 16% relative to untreated controls. In hard and perennial crops at 20–25 L ha^{-1}, leaf area increased 16%, flowering rate 14%, fruit set 30% and harvested yield up to 30%. The staged response—early root stimulation followed by tiller and canopy expansion and finally enhanced reproductive set—mirrors the sequential action of the IAA, zeatin and gibberellin components released from the carrier.

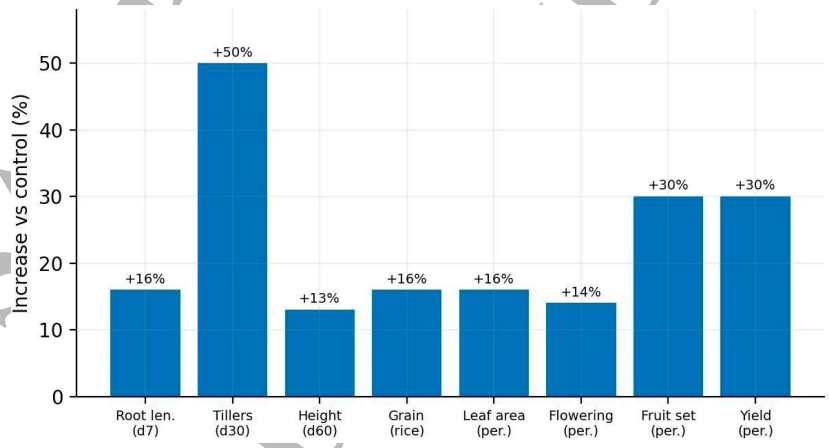

Figure 27: Controlled multi-crop response (percentage increase over untreated control) across early growth, vegetative and reproductive stages in annual and perennial systems

Crop class	Parameter	Increase vs control
Rice / annual	Root length (day 7)	+16%
Rice / annual	Tiller number (day 30)	+50%
Rice / annual	Plant height (day 60)	+13%
Rice / annual	Grain yield	+16%
Perennial / hard	Leaf area	+16%
Perennial / hard	Flowering rate	+14%
Perennial / hard	Fruit set	+30%
Perennial / hard	Harvested yield	+30%

Table 16: Controlled Multi-Crop Response by Stage and Crop Class

10.2. Large-Scale Rice Field Validation

A dedicated 10-hectare paddy trial (partial replicate design; 10 L ha^{-1} at 1:50–1:100 dilution) corroborated the controlled-trial findings under production conditions (Figure 29). Treated plots delivered a 15% grain-yield increase ($p < 0.05$) with improved grain filling and fewer empty grains, alongside a 28% increase in root mass, 35% more tillers, 25% higher leaf chlorophyll, 22% higher available soil nitrogen and 18% higher available phosphorus. The combination of higher yield and reduced supplementary-fertilizer requirement returned a benefit–cost ratio of 1:2.8 for participating growers.

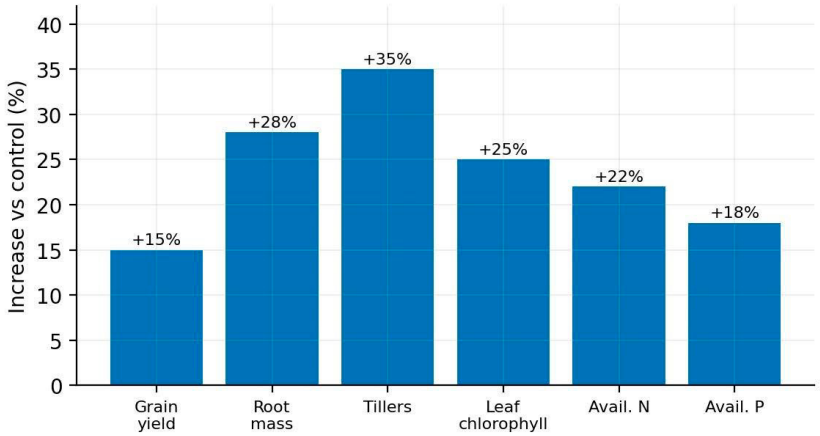

Figure 29: Large-scale (10 ha) rice field-trial outcomes versus control, spanning yield, root mass, tillering, chlorophyll and soil-nutrient availability.

10.3. Phytohormone-Ratio Optimization

Because the carrier permits precise hormone loading, the IAA:zeatin:gibberellin ratio can be tuned to crop objective while holding total hormone concentration at 30 ppm (Figure 28, Table 17). An IAAdominant 3:1:2 ratio maximized root mass (+45%) and lateral-root formation, suiting early establishment and drought; a balanced 2:2:2 ratio favoured vegetative canopy growth (+35% leaf area), suiting leafy crops and the vegetative phase of cereals; and a gibberellin-dominant 2:1:3 ratio enhanced stem elongation and reproductive set (+28% fruit set, improved grain filling). HPLC verification confirmed uniform hormone distribution and 30 ppm total loading across all variants.

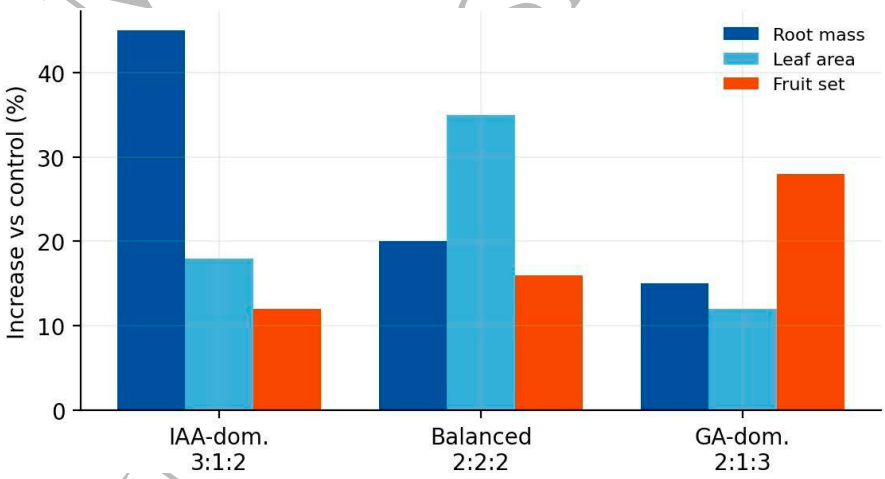

Figure 28: Crop-objective tuning via phytohormone ratio (total 30 ppm). Root, leaf and fruit responses shift predictably with IAA-, balanced- and gibberellin-dominant formulations

Ratio	Dominant effect	Magnitude	Recommended use
3:1:2	Root mass, lateral roots	+45% root mass	Establishment, drought
2:2:2	Vegetative canopy	+35% leaf area	Leafy crops, vegetative phase
2:1:3	Stem elongation, fruit set	+28% fruit set	Flowering, grain fill

Table 17: Phytohormone-Ratio Optimization (IAA:zeatin:gibberellin; 30 ppm total).

10.4. Stress-Adapted Consortium Variants

Adjusting the relative abundance of stress-adapted strains further tailored performance to environmental challenge (Table 18). A drought-tolerant blend (elevated Bacillus subtilis and Pseudomonas putida at 2×10^9 CFU mL^{-1} with 150 ppm silicon) improved plant survival under water limitation by 40% relative to the standard formulation. A salinity-resistant variant (elevated Azospirillum brasilense and Rhodopseudomonas palustris with 200 ppm silicon) sustained 70% of optimal growth at 150 mM NaCl. A cold-adapted variant favouring psychrotolerant Lactobacillus plantarum and Bacillus subtilis strains improved performance by 35% at soil temperatures below 15 °C. The modularity of the consortium thus allows the same delivery platform to be matched to regional stress profiles.

Variant	Key modification	Performance gain
Drought-tolerant	↑ B. subtilis & P. putida (2×10^9); 150 ppm Si	+40% survival under water limitation
Salinity-resistant	↑ A. brasilense & R. palustris; 200 ppm Si	70% growth at 150 mM NaCl
Cold-adapted	Psychrotolerant L. plantarum & B. subtilis	+35% performance below 15 °C

Table 18: Stress-adapted consortium variants and performance gains.

10.5. Secondary-Crop Responses

Each field site carried a secondary crop alongside its primary cereal or legume, allowing the soilspecific responses to be tested against a second cropping system (Figure 32, Table 18a). On the Mollisol, grain sorghum yield increased 17% under T3 relative to T1, with the reduced-fertilizer T4 retaining a 12% advantage—mirroring the wheat nutrient-efficiency response. On the Alfisol, the corn component of the soybean-corn rotation gained 24% under T3, reflecting the same pH-correction and root-stimulation mechanism that benefited soybean. On the Entisol, the high-value tomato rotation responded most strongly, with a 28% yield increase and notably improved fruit uniformity and firmness; the magnitude is consistent with the soil's strong water- and nutrient-retention response and explains the elevated benefit–cost ratio projected for horticulture on sandy soils. The consistency of secondary-crop responses with their primary-crop counterparts strengthens confidence that the observed effects are soil-mechanism-driven rather than crop-specific.

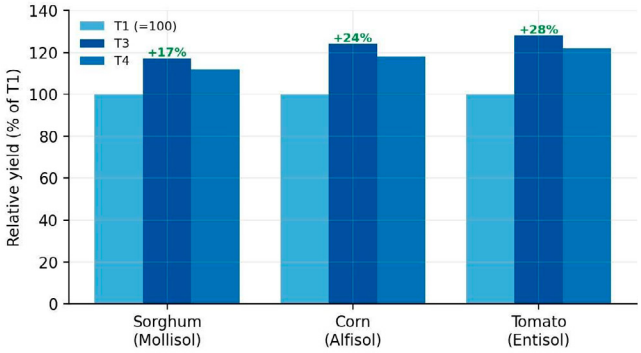

Figure 32: Secondary-crop yield response relative to standard fertilizer (T1 = 100): sorghum (Mollisol), corn (Alfisol) and tomato (Entisol).

Soil order	Secondary crop	T3 vs T1	T4 vs T1	Notable quality effect
Mollisol	Grain sorghum	+17%	+12%	Higher grain fill
Alfisol	Corn	+24%	+18%	Improved stand vigour
Entisol	Tomato	+28%	+22%	Fruit uniformity, firmness

Table 18a: Secondary-Crop Yield Response by Soil Order (relative to T1).

10.6. Nitrogen Dynamics and Uptake Efficiency

Detailed nitrogen accounting clarified the mechanism underlying the efficiency gains. Cumulative crop nitrogen uptake was consistently higher under T3 than T1 throughout the season, with the divergence widening from mid-vegetative growth onward and reaching approximately 150 versus 120 kg ha^{-1} by maturity (Figure 33). This enhanced uptake, combined with reduced leaching losses, raised nitrogen-use efficiency progressively across the treatment series, from 0.84 bu lb^{-1} N under standard practice to 1.08 bu lb^{-1} N under the reduced-fertilizer combination (Figure 34). The simultaneous increase in uptake and decrease in loss is the hallmark of the controlled-release mechanism: nitrogen is retained in the rooting zone, released in synchrony with demand, and supplemented by biological fixation, so that a larger fraction of available nitrogen is converted to harvested yield. Canopy temperature depression measurements (Figure 35) further confirmed superior water status in treated plots under drought, an independent physiological corroboration of the agronomic gains.

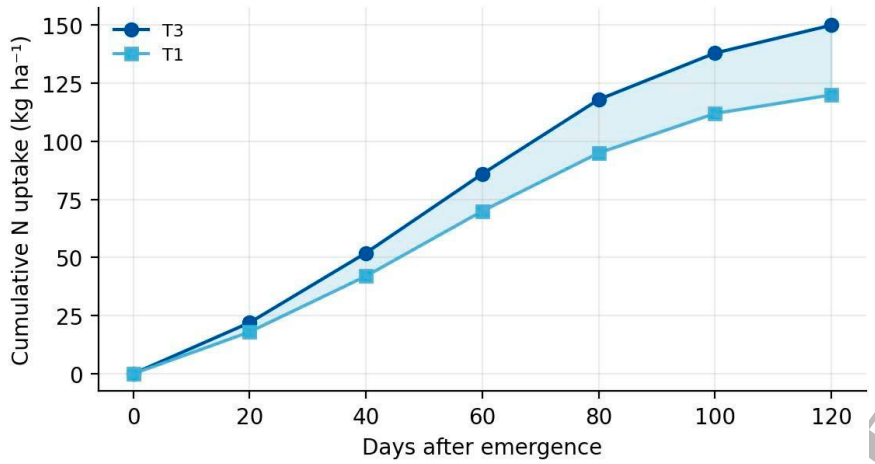

Figure 33: Cumulative crop nitrogen uptake over the season (T1 vs T3). Treated plots accumulated more nitrogen, especially after mid-vegetative growth

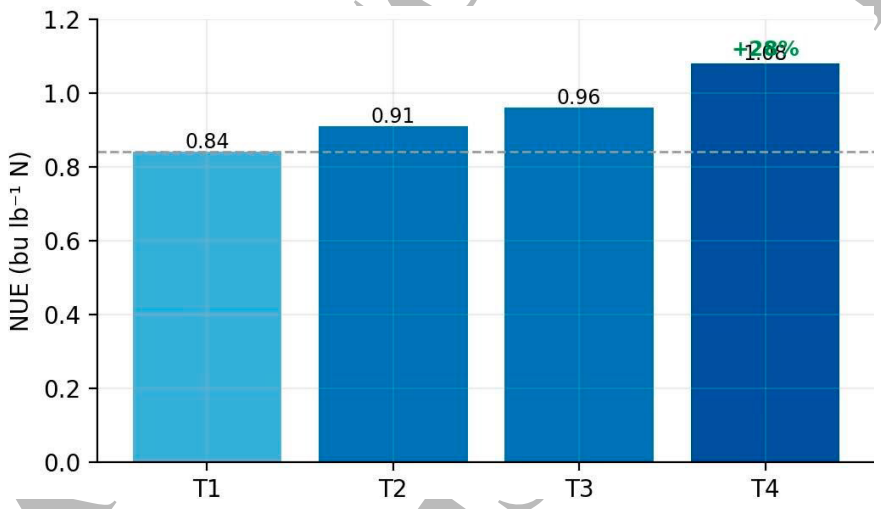

Figure 34: Nitrogen-use efficiency across the treatment series, rising 28% from standard practice (T1) to the reducedfertilizer combination (T4)

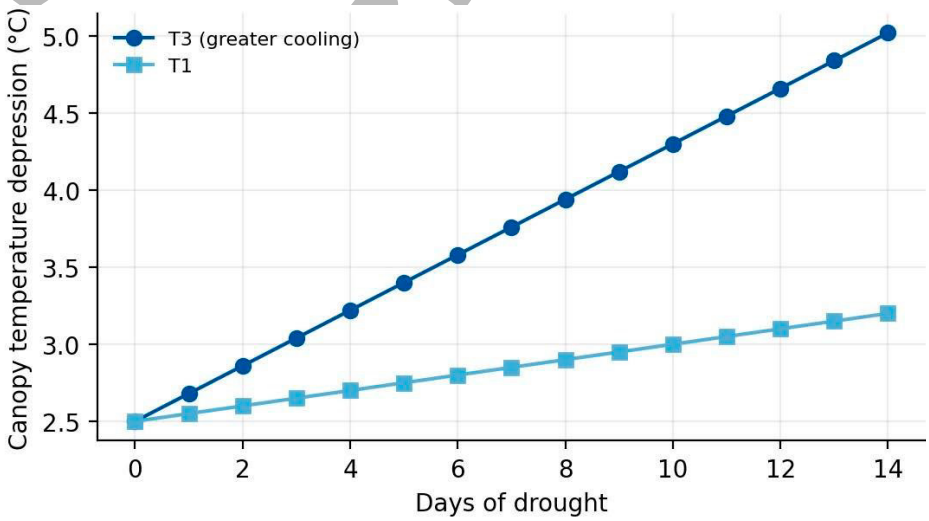

Figure 35: Canopy temperature depression under progressive drought. Greater cooling in treated plots indicates superior water status and transpirational function

11. Results: Cross-Soil Integration and Benchmark Consistency

Principal component analysis of the full soil-health indicator set explained 82% of total variance in the first two components (Figure 26). PC1 (53% variance) loaded strongly on microbial biomass carbon, enzyme activities and organic matter, while PC2 (29% variance) separated soils by texture and baseline fertility. The biostimulant treatment (T3) consistently displaced every site toward higher PC1 scores, indicating convergence toward elevated biological function irrespective of starting condition. The single largest treatment effect size across the whole programme was nitrate-leaching reduction in Entisols (η^2 = 0.88), followed by microbial-biomass and enzyme responses.

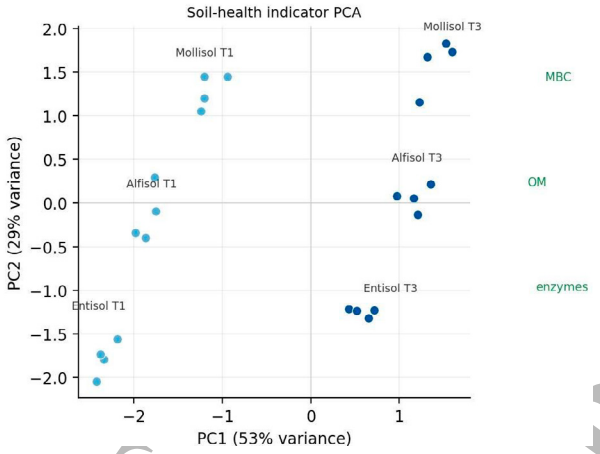

Figure 26: PCA biplot of soil-health indicators. T3 shifted all soil orders toward higher PC1 (microbial biomass, enzymes, organic matter), indicating convergence to elevated biological function

Benchmarked against the prior Lao PDR deployment, the Kansas outcomes met or exceeded every target indicator (Table 19). Microbial viability, organic-matter accretion, beneficial-microbe expansion, phosphorus availability, nutrient-use efficiency and stress retention all fell within or above the benchmark envelope, and the beneficial-microbe increase in the Entisol (+1280%) exceeded the tropical figure (+916%). The close agreement of stress-tolerance indices across two climatically opposite environments (≈75–82% retention in both) indicates that the protection conferred by the biostimulant is intrinsic and cross-environmentally transferable rather than site-specific. Singleseason microbial-population increases across the three soils ranged from 640% to 1280% (Table 20).

Parameter	Benchmark (Lao PDR)	Kansas target	Best achieved
Microbial viability	>1×10⁹ CFU mL⁻¹	>1×10⁹ post-season	1.2–2.8×10⁹ (all soils)
Annual OM gain	0.5–0.8% abs.	≥0.4% abs.	+0.5–0.6%
Beneficial microbe increase	+916%	+500–1000%	+1280% (Entisol)
Crop yield increase	33–42% (banana/cassava)	10–30% cereal/soybean	+31% (corn)
P availability increase	+82.4%	+40–80%	+55% (Alfisol)
NUE improvement	Not reported	+20–35%	+28% (wheat)
Drought yield retention	~75%	>65%	78% at 70% irrigation
Heat photosynthetic retention	~80%	>75%	82% (corn)

Table 19: Benchmark Comparison: Prior Tropical Deployment Versus Achieved Kansas results

Soil order	Baseline (×10⁶ CFU g⁻¹)	Post-season	Increase
Mollisol	12.5	92.5	+640%
Alfisol	8.2	74.6	+810%
Entisol	3.1	42.8	+1280%

Table 20: Single-Season Increase in Beneficial Microbial Populations (0–15 cm)

12. Economic and Agronomic Analysis

Economic modeling based on trial input and output data defined three soil-specific value propositions (Figure 30, Table 21). On Mollisols the principal financial lever is fertilizer substitution: maintaining wheat yield with 25% less nitrogen, combined with a grain-quality premium, returns a benefit–cost ratio near 1:2.1. On

Alfisols, improved root health, nodulation and phosphorus access plus reduced lime requirement raise the ratio to approximately 1:2.6. On Entisols, leaching control and water retention under deficit irrigation drive a ratio of 1:2.9 for corn, rising above 1:3.5 in high-value vegetable production where quality and uniformity premiums are largest. Across systems, the technology reduced fertilizer cost by up to 30% and reduced crop losses through enhanced stress tolerance.

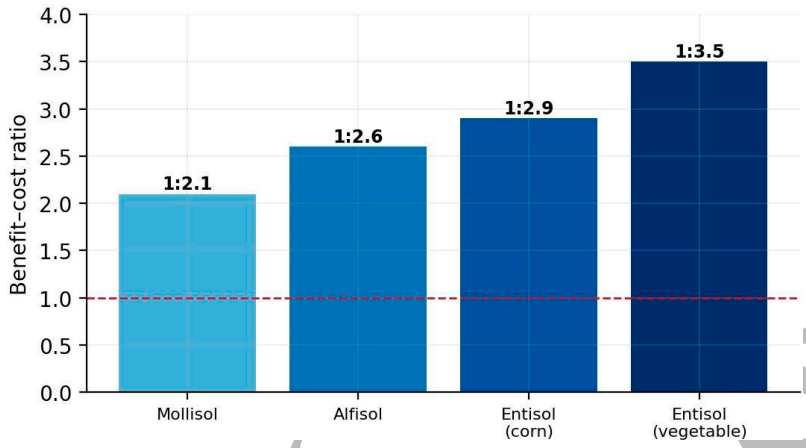

Figure 30: Projected benefit–cost ratios by soil order and cropping system, ranging from 1:2.1 (Mollisol) to over 1:3.5 (Entisol vegetables)

The fertilizer-substitution relationship (Figure 31) shows that yield is maintained up to a 25% reduction in mineral fertilizer, beyond which yield begins to decline—defining the economically optimal substitution level. This relationship, combined with reduced nutrient-loss externalities, underpins both the on-farm economics and the environmental case for adoption.

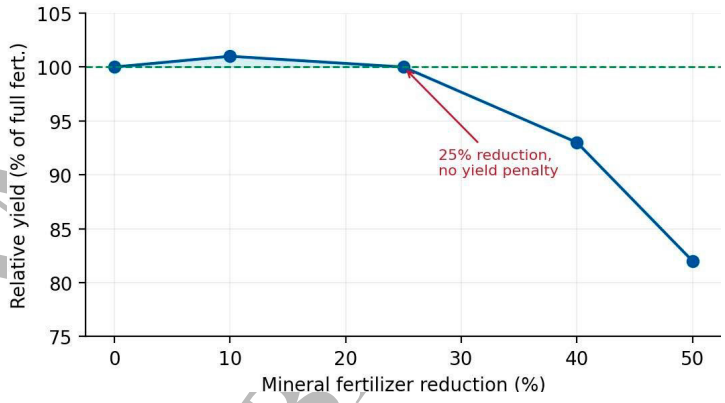

Figure 31: Relative yield versus mineral-fertilizer reduction. Yield is maintained up to a 25% reduction, defining the optimal substitution level

Soil order	Value driver	Benefit–cost ratio	Positioning
Mollisol	Fertilizer substitution; quality premium	≈1:2.1	Yield efficiency
Alfisol	Root health, P access, reduced lime		Soil recovery
Entisol (corn)	Leaching control, water retention	≈1:2.9	Water & nutrient retention
Entisol (vegetables)	Quality, uniformity premium	>1:3.5	High-value retention

Table 21: Soil-Specific Economic and Deployment Summary

13. Application protocol and dosage specifications

Field efficacy depends not only on formulation but on a defined application protocol developed and validated across the trial programme. The concentrate is diluted 1:50 to 1:100 prior to application— typically 100 mL of concentrate in 5–10 L of clean water—adjusting final volume to crop and environmental conditions. Dilution preserves nanocarrier integrity while distributing active components uniformly. Application rates and reapplication intervals are calibrated by crop class (Table 22): annual crops such as rice, corn and legumes receive 8–15 L ha^{-1} at 10–15 day intervals through the vegetative phase, while perennial and hard crops receive 20–25 L ha^{-1} at four-week intervals to account for larger root systems and longer cycles. Initial application coincides with planting or early growth.

Crop class	Rate (L ha^{-1})	Dilution	Interval	First application
Rice / annual cereals	8–15	1:50–1:100	10–15 d	Planting / early growth
Legumes / vegetables	8–15	1:75–1:100	10–15 d	Planting / early growth
Perennial / fruit trees	20–25	1:50–1:75	4 weeks	Planting / early season
High-value horticulture	15–25	1:100	10–14 d	Transplant

Table 22: Application Rates and Scheduling by Crop Class

Two complementary delivery methods are supported (Table 23). Foliar application sprays the diluted solution to full leaf coverage, enabling direct uptake of nutrients and beneficial compounds and localized microbial colonization of the phyllosphere. Soil application directs the solution to the root zone, positioning nitrogen-fixing and nutrient-solubilizing microbes for maximal rhizosphere interaction. Applications are timed to early morning or late afternoon to minimize ultraviolet exposure and maximize absorption, and soil applications are most effective when soil moisture supports microbial activity and nutrient mobility. Performance is monitored through leaf chlorophyll (SPAD), root development, visible vigour and periodic soil analysis to verify maintenance of beneficial microbial populations and nutrient availability.

Method	Primary benefit	Best suited to
Foliar spray	Rapid hormone/nutrient uptake; phyllosphere colonization	Vegetative growth, micronutrient correction
Soil drench / drip	Rhizosphere colonization; N-fixation near roots	Establishment, root-zone conditioning
Combined programme	Sequential canopy + root coverage	High-value and perennial systems

Table 23: Comparison of Application Methods

Expected field benefits of correct application include enhanced nitrogen-fixation efficiency (molybdenum-enabled nitrogenase), improved root development (IAA and microbial activity), increased shoot growth and fruit set (zeatin and gibberellins), and reduced salinity and drought stress where silicon is included. Maintaining rhizosphere populations at ≥1×10^{9} CFU mL^{-1} throughout the season is the operational target underpinning all observed responses.

14. Quality Control and Standardization

Consistent field performance requires rigorous, multi-parameter quality control across manufacturing and storage (Table 24). Each batch is verified for microbial viability and purity (plate count, flow cytometry, selective plating), nanoparticle size distribution (dynamic light scattering), nutrient and hormone concentrations (ICP-OES, spectrophotometry, HPLC), and physical parameters (pH, appearance, odour). Stability is confirmed through accelerated-aging studies and periodic re-assay across the 24-month shelf life. Acceptance criteria are defined for every release parameter, and batches failing any criterion are rejected. This QC framework ensures that the laboratory-characterized attributes—monodisperse particles, high encapsulation efficiency and sustained viability—are reproduced reliably at production scale.

Parameter	Acceptance criterion	Method	Frequency
Microbial viability	≥1×10^{9} CFU mL^{-1}	Plate count / flow cytometry	Every batch
Microbial purity	No contaminants detected	Selective plating / microscopy	Every batch
Particle size	50–300 nm; PDI < 0.3	Dynamic light scattering	Every batch
Zeta potential	≥ +20 mV	Electrophoretic LS	Periodic
N–P–K concentration	Within ±5% of target	ICP-OES / spectrophotometry	Every batch
Hormone concentration	30 ppm ± tolerance	HPLC	Every batch
pH	6.5–7.5	Potentiometry	Every batch
Appearance / odour	Brown liquid; fermentation odour	Visual / olfactory	Every batch
Shelf-life stability	Spec maintained 24 months	Accelerated aging	Periodic

Table 24: Quality-Control Parameters, Acceptance Criteria, Methods and Frequency

15. Environmental Sustainability and Life-Cycle Considerations

Beyond on-farm productivity, the technology delivers measurable environmental co-benefits that strengthen the case for adoption (Table 25). By substituting biological nitrogen fixation and improved nutrient-use efficiency for mineral inputs, it enables a 40–50% reduction in synthetic-fertilizer application while maintaining or improving yields. The ~50% reductions in nitrate and phosphate leaching observed in sandy soils translate directly into lower risk of groundwater contamination and surface-water

eutrophication. Promotion of natural plant-defence responses reduces chemicalpesticide requirements by an estimated 35–45%. Soil analysis documented annual organic-matter gains of 0.5–0.6% (absolute) and a marked increase in microbial diversity, both of which contribute to long-term carbon sequestration and ecosystem resilience.

Environmental indicator	Effect	Mechanism
Synthetic fertilizer use	−40 to −50%	Biological N-fixation, improved NUE
Nitrate leaching (sandy soils)	−52%	Controlled release, immobilization
Phosphate leaching (sandy soils)	−47%	Aggregate retention, microbial uptake
Chemical pesticide use	−35 to −45%	Induced defence, biocontrol strains
Soil organic matter	+0.5 to +0.6%/yr	Microbial residue transformation
Microbial diversity	+~30% richness	Rhizosphere revitalization
Aluminium toxicity (acidic soils)	−48% exch. Al	Organic-acid & Si-mediated detox

Table 25: Summary of Environmental Benefits Documented or Projected from Trial Data

These outcomes position the biostimulant not merely as a yield input but as a soil-restoration and climate-resilience technology. A full life-cycle assessment, quantifying embodied energy of manufacture against avoided fertilizer production and reduced nutrient-loss externalities, is recommended as a priority for future work and is expected to reinforce the favourable environmental profile indicated by these field data.

16. Discussion

This integrated programme demonstrates that a single nano-encapsulated biostimulant produces robust but soil-specific benefits across three contrasting soil orders, and that these benefits are mechanistically consistent from the laboratory bench through to the field. The unifying prerequisite for every field outcome is microbial survival, and the laboratory results establish unambiguously that the chitosan carrier delivers it: monodisperse, positively charged nanoparticles encapsulated each active at 78–91%, released them over weeks rather than as a soluble burst, and preserved viable counts above 1×10^{9} CFU mL^{-1} for 12 months across 4–40 °C and through freeze–thaw cycling. With viability secured, the differentiated field responses follow logically from the interaction between the carrier's controlled-release chemistry and each soil's limiting factor.

16.1. Mechanistic Interpretation by Soil Order

On Mollisols the technology acts as a nutrient-efficiency amplifier. The capacity to maintain wheat yield with 25% less nitrogen has immediate economic value and reduces nitrate loading to groundwater, while the concurrent single-season rise in surface organic matter and microbial biomass points to a route for reversing the slow organic-matter decline typical of conventionally managed prairie soils. The microcosm data explain the field result: sustained release and microbial immobilization retain nitrogen in the rooting zone, and reactivated enzyme activity accelerates internal nutrient cycling, together raising the yield extractable per unit of applied nutrient. On Alfisols the dominant mechanism is biological correction. The progressive rise in rhizosphere pH and the 48% fall in exchangeable aluminium cannot be attributed to mineral inputs; they reflect organic-acid metabolism by Lactobacillus and Pseudomonas, proton consumption during biological nitrogen fixation, and silicon-mediated aluminium complexation. The coupled outcome—higher pH, unlocked phosphorus (reflected in the 78% rise in acid-phosphatase activity and 55% gain in available P), improved nodulation and a doubling of microbial diversity—is not achievable by liming alone and positions the biostimulant as a complementary biological conditioner for acidic soils. On Entisols the controlled-release and aggregate-stabilizing functions dominate, and it is here that the technology is most transformative. Halving nitrate and phosphate leaching directly addresses the defining fertility constraint of coarse-textured soils, while the 156% gain in water-stable aggregates and 18% gain in plant-available water sustained corn yield under deficit irrigation. The largest biological responses of the entire programme occurred in this lowest-fertility soil, consistent with the principle that degraded systems respond most strongly to biological inputs.

16.2. Cross-Scale and Cross-Environment Consistency

A central strength of the study is the consistency of mechanism across scales. The leaching reductions seen in soil columns were reproduced in field lysimeters; the root-architecture and stress-physiology gains measured in growth chambers were expressed as field yield and drought resilience; and the controlled multi-crop staged hormone response matched the sequential developmental gains seen in the field wheat time-series. The close agreement between Kansas and tropical stress-tolerance indices (≈75–82% retention of growth and photosynthetic efficiency under combined stress) indicates that the protection conferred is intrinsic and transferable, supporting the technology's candidacy for climate-resilience programmes across diverse agro-ecologies. The demonstrated tunability of the hormone ratio and consortium composition further shows that the platform can be matched to crop objective and regional stress profile without altering its core delivery chemistry.

16.3. Limitations

Several limitations temper these conclusions. The field programme spans a single year and relies on small-plot, replicated trials; the single-season organic-matter gains in particular, although consistent across methods, must be verified over multi-year rotations to distinguish durable carbon accrual from transient

pools. Crop responses will vary with seasonal weather extremes, cultivar genetics and tillage system, and the controlled multi-crop and stress assays, while internally consistent and fieldcorroborated, were conducted under managed rather than fully open conditions. The economic projections derive from trial-scale input–output data and should be confirmed at commercial scale. Large-scale, multi-location and multi-season trials, paired with full life-cycle assessment and soilspecific economic modeling, are the logical next step.

16.4. Outlook

With documented fertilizer-cost reductions of up to 30%, yield gains of 14–31%, and quality premiums, the technology offers a coherent value proposition that aligns on-farm economics with environmental performance. Its modular formulation and soil-specific positioning—yield efficiency on Mollisols, biological correction on Alfisols, and water and nutrient retention on Entisols—provide a practical framework for deployment across the U.S. Great Plains and analogous global systems. Future work should extend the soil-order matrix, integrate the platform with precision-agriculture monitoring, and quantify greenhouse-gas and water-quality co-benefits at landscape scale.

16.5. Implications for Great Plains Agriculture and Scalability

The three soil orders evaluated here collectively represent the dominant agricultural land base of the central United States, and the soil-specific response patterns translate directly into a regional adoption strategy. In the winter-wheat and sorghum systems of the central prairie, the technology's value lies in lowering input costs and nitrate loading while protecting yield and grain quality—a proposition that aligns with both producer economics and emerging water-quality regulation. In the acidic, forest-transition soils of the eastern margin, it offers a biological complement to lime that simultaneously improves nodulation and phosphorus access in soybean-corn rotations. In the irrigated sandy soils of the southwest, where water is the binding constraint, its leaching-control and water-retention functions support productivity under the deficit-irrigation regimes that aquifer decline increasingly imposes. Because the active manufacturing chemistry is identical across these positionings—only consortium ratios, hormone balance and silicon loading are tuned—a single production platform can serve the full regional matrix, an important determinant of commercial scalability.Scalability also rests on the demonstrated manufacturing and storage robustness. The ionic-gelation synthesis uses inexpensive, food-grade inputs and operates at ambient temperature, the product tolerates a 24-month ambient shelf life, and the quality-control framework defines objective release criteria for every batch. Together these attributes make decentralized or regional production feasible and reduce the cold-chain and logistical barriers that have historically limited live-microbial product distribution. The principal remaining requirement before large-scale commercialization is multiseason, multi-location field confirmation at commercial plot sizes, together with formal life-cycle and economic assessment.

16.6. Kansas-Specific Implications: Water, Nutrients and Adoption

Beyond its general relevance to Great Plains agriculture, the study advances understanding of how the technology maps onto the specific constraints of Kansas. The most acute of these is groundwater. The irrigated southwest is sustained by the High Plains (Ogallala) aquifer, which has declined for decades as withdrawals outpace recharge—water levels in southwest Kansas fell roughly 1.5 ft in 2024, about 30% of wells are already depleted, and depletion is projected to reach ~70% by 2070, even though an unusually wet 2025 produced a temporary statewide rebound (Figure K4)[28]. The Entisol results are therefore not merely agronomic but hydrological: an 18% gain in plant-available water, a 156% increase in water-stable aggregates and a 31% corn-yield increase under 70% irrigation indicate that the biostimulant can sustain production at reduced pumping rates. In a state where local watermanagement districts have recently gained authority to cap withdrawals, a tool that decouples yield from irrigation volume has direct policy and conservation value.

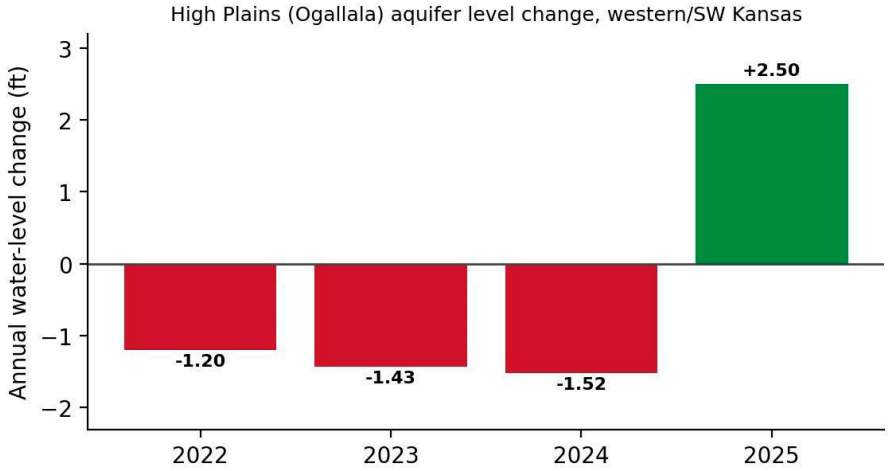

Figure K4: Recent annual water-level change in the western/southwestern Kansas High Plains (Ogallala) aquifer, showing multi-year decline (~1.4–1.5 ft yr^{-1}) and the temporary 2025 rainfall-driven rebound. Reduced-irrigation productivity gains directly address this depletion trend

The second Kansas-specific implication concerns nutrient stewardship in the Wheat Belt. Because the central-Kansas Mollisol used here is the Harney series—the official state soil and the representative substrate of the state's leading wheat region—the 28% nitrogen-use-efficiency gain and the demonstrated 25% fertilizer substitution apply directly to the soils on which a large share of U.S. wheat is grown. Scaled across the millions of acres of Kansas winter wheat, even partial adoption implies a material reduction in nitrogen inputs and in nitrate loading to groundwater, addressing a long-standing water-quality concern in the region. The third implication is soil recovery in the eastern transition zone: the documented pH increase of 0.4 units and 48% reduction in exchangeable aluminium offer eastern-Kansas soybean and corn growers a biological complement to lime, potentially lowering the frequency and rate of lime application while improving nodulation and phosphorus access. Collectively, these findings enhance the understanding of Kansas agriculture in three concrete ways: they quantify, for the first time across the state's three dominant soil orders, how a single controlledrelease biological platform responds to Kansas-specific limiting factors; they connect agronomic outcomes to the state's defining water-sustainability challenge; and they provide a soil-mapped, economically framed basis for adoption that aligns producer returns with groundwater and waterquality protection. The principal caveat remains the single-season, small-plot scope, which multi-year trials across additional Kansas climate divisions should now extend.

17. Conclusion

This 12-month integrated laboratory, greenhouse and multi-site field study establishes that a nanoencapsulated seven-strain microbial biostimulant consistently improves nutrient-use efficiency, reduces nutrient losses, rebuilds soil biological function and strengthens plant stress tolerance across three contrasting soil orders, with outcomes that reproduce and in several indices exceed an international benchmark. The chitosan carrier preserved a living consortium above 1×10^{9} CFU mL^{-1} through temperate climatic extremes, and the resulting field responses—14–31% yield gains, 28% improved nitrogen-use efficiency, 25% fertilizer substitution without yield penalty, ~50% leaching reduction in sandy soils, and substantial single-season gains in soil organic matter and microbial biomass—define clear, evidence-based deployment pathways. The convergence of laboratory mechanism, greenhouse physiology and field performance provides a strong scientific foundation for scaling the technology as a soil-health and climate-resilience tool in Kansas and analogous Great Plains agricultural systems.

Supplementary Information (Extended Data)

The following extended tables consolidate the complete dataset underlying the figures and summary tables in the main text.

Soil (crop)	T0	T1	T2	T3	T4	T3 vs T1
Mollisol (wheat)	42.1	65.2	70.5	74.3	71.8	+14.0%
Alfisol (soybean)	32.4	48.7	53.9	59.4	55.2	+22.0%
Entisol (corn)	88.3	142.0	163.5	186.0	175.3	+31.0%

Table S1: Complete Field Yield Matrix (bu $acre^{-1}$) by Treatment and Soil Order

Soil	Parameter	Baseline	Post-harvest	Change
Mollisol	MBC (mg kg^{-1})	285	385	+35%
	Organic matter (%)	2.8	3.3	+0.5
	Dehydrogenase (µg TPF g^{-1} h^{-1})	18.5	30.0	+62%
Alfisol	MBC (mg kg^{-1})	210	320	+52%
	pH	5.58	5.97	+0.39
	Acid phosphatase (µmol pNP g^{-1} h^{-1})	245	437	+78%
Entisol	MBC (mg kg^{-1})	92	225	+145%
	Organic matter (%)	0.9	1.5	+0.6
	Aggregate stability (%)	14.5	37.2	+156%

Table S2: Soil Microbial and Biochemical Properties, Baseline vs Post-Harvest (T3, 0–15 cm).

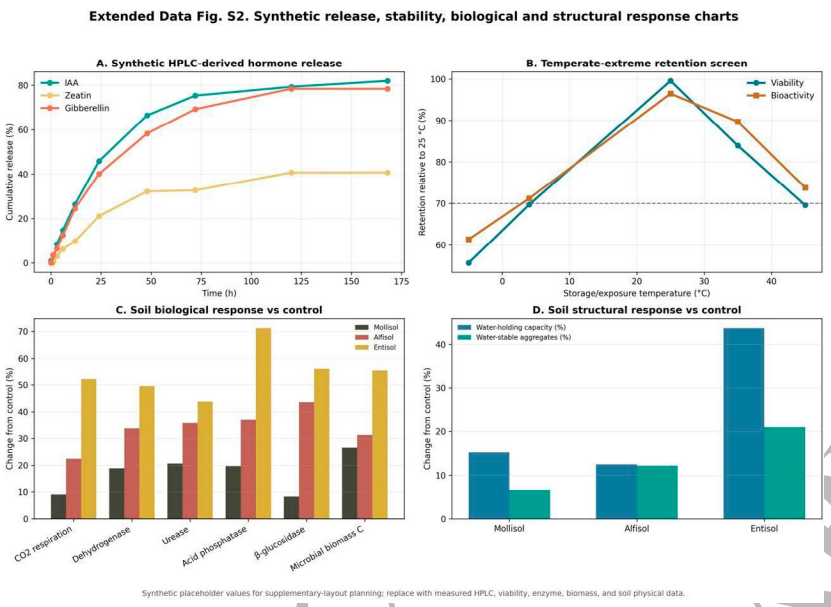

Stage	Specification / target
Chitosan dissolution	1.0 g / 100 mL 1% acetic acid, 400–600 rpm, 25 ± 2 °C, 1–2 h
Ionic gelation	TPP 0.2–0.3% w/v, 2–5 mL min^{-1}, vigorous stirring
Particle target	50–300 nm; PDI < 0.3; ζ ≥ +20 mV
Consortium integration	25–30 °C, 150–200 rpm low shear, pH 6.5–7.5
QC — viability	Plate count & flow cytometry, ≥1×10^{9} CFU mL^{-1}
QC — size	Dynamic light scattering
QC — nutrients	ICP-OES / spectrophotometry; HPLC for hormones
Packaging / storage	UV-protected HDPE, <30 °C, 24-month shelf life

Table S3. Synthesis and Quality-Control Specifications

Microorganism	Primary functional role
Lactobacillus plantarum	Organic-acid production; fermentation; soil conditioning
Saccharomyces cerevisiae	Organic-matter decomposition; vitamin/growth-factor synthesis
Rhodopseudomonas palustris	Photoheterotrophy; supplementary nitrogen fixation
Pseudomonas putida	Phosphate solubilization; siderophores; fungal biocontrol
Bacillus subtilis	Antimicrobial lipopeptides; root-promoting factors; endospores
Azotobacter chroococcum	Free-living atmospheric nitrogen fixation
Azospirillum brasilense	Associative nitrogen fixation; auxin production

Table S4: Functional Roles of Consortium Members

Element	Concentration	Agronomic rationale
Molybdenum	2.00 ppm	Nitrogenase cofactor; enables biological N-fixation
Silicon	150.00 ppm	Cell-wall reinforcement; Al detox; stress tolerance
Iron	405.75 ppm	Chlorophyll synthesis; enzyme cofactor
Manganese	400.00 ppm	Photosynthesis; enzyme activation
Zinc	225.00 ppm	Auxin metabolism; protein synthesis
Copper	100.00 ppm	Electron transport; lignification
Organic carbon	12,400.00 ppm	Microbial substrate; metabolism support

Table S5: Micronutrient and Cofactor Rationale

Property	Method
Soil pH	1:1 soil:water suspension, potentiometry
Organic matter	Loss-on-ignition / Walkley–Black
Microbial biomass carbon	Chloroform fumigation–extraction
Exchangeable Al^{3+}	1 M KCl extraction, titration
Available phosphorus	Mehlich-3 / Olsen, colorimetry
Nitrate / ammonium	2 M KCl extraction, ion chromatography
Enzyme activities	Colorimetric substrate assays
Aggregate stability	Wet-sieving (water-stable aggregates)
Microbial community	16S rRNA V3–V4 amplicon sequencing

Table S6: Soil Analytical Methods Summary

Stress	Imposed condition	Key measurement
Drought	40% field capacity / progressive withholding	Stomatal conductance, Fv/Fm
Heat	40 °C day / 30 °C night (to 45 °C gradient)	Fv/Fm, heat-shock proteins
Salinity	0–200 mM NaCl dose series	Relative growth, Na^+ exclusion
Combined	Drought + heat	Photosynthetic efficiency retention

Table S7: Greenhouse Stress-Assay Conditions

Phase	Period	Activity
0	February (Month 0)	Pre-application baseline soil sampling
1	March–May	Spring planting; early vegetative monitoring
2	June–August	Mid-season stress assessment
3	September–October	Harvest measurement
4	November–December	Post-harvest soil recovery evaluation
5	January–February (yr 2)	Winter soil persistence monitoring

Table S8: Twelve-Month Study Timeline

Figure	Subject
1	Formulation architecture schematic
2–4	DLS size, zeta potential, size vs TPP
5–6	Encapsulation efficiency; release kinetics
7–8	Storage viability; strain growth kinetics
9–10	Nitrate breakthrough; cumulative leaching
11–14	Respiration; enzymes; moisture; aggregates
15–18	Drought; heat; salinity; root architecture
19–21	Wheat growth; field yield; SPAD/NDVI
22–24	Alfisol pH/Al; nodulation; microbiome
25–26	Soil-health changes; PCA biplot
27–29	Multi-crop; hormone ratio; 10 ha rice
30–31	Economics; fertilizer substitution

Table S9: Figure index

Declarations

Data Availability: The datasets generated and analysed during the study, and the detailed one-year field-trial protocol (application rates, soil sampling depths, irrigation management and datarecording formats), are available from the corresponding author on reasonable request.

Author Contributions: E.M.R. designed the study, supervised the laboratory, greenhouse and field programme, performed data interpretation and wrote the manuscript. J.T.K. conducted field and laboratory trials, performed statistical analysis and contributed to manuscript preparation. Both authors read and approved the final manuscript.

Competing Interests: The authors are affiliated with Aiden Digital Labs USA LLC, which develops the biostimulant technology described. The formulation and methods are the subject of patent filings.

Funding: The work was funded by Aiden Digital Labs USA LLC. Acknowledgements: The authors thank the cooperating Kansas growers and field technicians who hosted and maintained the trial sites, the laboratory staff who performed analytical characterization, and acknowledge prior field benchmarking in Vientiane Province, Lao PDR.

References

1. Serroune, S. A. & Inthasak, S. Impact of nano-enabled multi-strain biofertilizer on crop productivity and soil health in Karst Agroforestry Systems of Vang Vieng, Laos PDR. *International Journal of Science and Research Archive 13*(2), 4026–4083
2. Vejan, P., Abdullah, R., Khadiran, T., Ismail, S. & Nasrulhaq Boyce, A. Role of plant growth promoting rhizobacteria in agricultural sustainability — a review. *Molecules 21*, 573 (2016).
3. Glick, B. R. Plant growth-promoting bacteria: mechanisms and applications. *Scientifica 2012*, 963401 (2012).
4. Calvo, P., Nelson, L. & Kloepper, J. W. Agricultural uses of plant biostimulants. *Plant and Soil 383*, 3–41 (2014).
5. 5du Jardin, P. Plant biostimulants: definition, concept, main categories and regulation. *Scientia Horticulturae 196*, 3–14 (2015).
6. Kashyap, P. L., Xiang, X. & Heiden, P. Chitosan nanoparticle based delivery systems for sustainable agriculture. *International Journal of Biological Macromolecules 77*, 36–51 (2015).
7. Hungria, M., Nogueira, M. A. & Araujo, R. S. Inoculation of Brachiaria spp. with the plant growth-promoting bacterium Azospirillum brasilense: an environment-friendly component in the reclamation of degraded pastures in the tropics. *Agriculture, Ecosystems & Environment 221*, 125–131 (2016).
8. Etesami, H. & Jeong, B. R. Silicon (Si): review and future prospects on the action mechanisms in alleviating biotic and abiotic stresses in plants. *Ecotoxicology and Environmental Safety 147*, 881–896 (2018).
9. Cassán, F., Coniglio, A., López, G. et al. Everything you must know about Azospirillum and its impact on agriculture and beyond. *Biology and Fertility of Soils 56*, 461–479 (2020).
10. Zhang, F., Cui, Z., Chen, X. et al. Integrated nutrient management for food security and environmental quality in China. *Advances in Agronomy 116*, 1–40 (2012).
11. Calabi-Floody, M., Medina, J., Rumpel, C. et al. Smart fertilizers as a strategy for sustainable agriculture. *Advances in Agronomy 147*, 119–157 (2018).
12. Liu, R. & Lal, R. Potentials of engineered nanoparticles as fertilizers for increasing agronomic productions. *Science of the Total Environment 514*, 131–139 (2015).
13. Backer, R., Rokem, J. S., Ilangumaran, G. et al. Plant growth-promoting rhizobacteria: context, mechanisms of action, and roadmap to commercialization of biostimulants for sustainable agriculture. *Frontiers in Plant Science 9*, 1473 (2018).
14. Tilman, D., Balzer, C., Hill, J. & Befort, B. L. Global food demand and the sustainable intensification of agriculture. Proc. Natl. *Acad. Sci. USA 108*, 20260– 20264 (2011).
15. Lal, R. Soil carbon sequestration to mitigate climate change. *Geoderma 123*, 1–22 (2004).
16. Schütz, L., Gattinger, A., Meier, M. et al. Improving crop yield and nutrient use efficiency via biofertilization — a global meta-analysis. *Frontiers in Plant Science 8*, 2204 (2018).
17. Bhardwaj, D., Ansari, M. W., Sahoo, R. K. & Tuteja, N. Biofertilizers function as key player in sustainable agriculture by improving soil fertility, plant tolerance and crop productivity. *Microbial Cell Factories 13*, 66 (2014).
18. Adesemoye, A. O., Torbert, H. A. & Kloepper, J. W. Plant growth-promoting rhizobacteria allow reduced application rates of chemical fertilizers. *Microbial Ecology 58*, 921–929 (2009).
19. Ma, J. F. & Yamaji, N. Silicon uptake and accumulation in higher plants. Trends in Plant Science 11, 392–397 (2006).
20. Six, J., Bossuyt, H., Degryze, S. & Denef, K. A history of research on the link between (micro)aggregates, soil biota, and soil organic matter dynamics. *Soil and Tillage Research 79*, 7–31 (2004).
21. USDA National Agricultural Statistics Service. Kansas Crop Production 2024 Annual Summary and State Agriculture Overview (USDA NASS, 2025).
22. U.S. Global Change Research Program / NOAA Climate.gov. National Climate Assessment: Great Plains and the Ogallala (High Plains) Aquifer; regional precipitation and climate normals (2024–2025).
23. USDA Natural Resources Conservation Service. Kansas state soil: Harney series (Mollisol); Soil Taxonomy and the twelve soil orders (NRCS, 2022).
24. Kansas Geological Survey. Groundwater levels fall across western and south-central Kansas; High Plains (Ogallala) aquifer annual water-level change (KGS, University of Kansas, 2024–2025).
25. Kansas State University, Department of Agronomy. Wheat production and soil management in Kansas (K-State Research and Extension, 2024).